Inorganic Chemistry

Article

pubs.acs.org/IC

Electronic Structures of Ruthenium and Osmium Complexes of 9,10-Phenanthrenequinone

Manas Kumar Biswas,[†] Sarat Chandra Patra,[†] Amarendra Nath Maity,[‡] Shyue-Chu Ke,[‡] Nirmal Das Adhikary,[§] and Prasanta Ghosh*[,†]

[†]Department of Chemistry, R. K. Mission Residential College, Narendrapur, Kolkata 103, India

[‡]Department of Physics, National Dong Hwa University, Shou-Feng, Hualien 97401, Taiwan

[§]Indian Institute of Chemical Biology, Jadavpur, Kolkata 32, India

Supporting Information

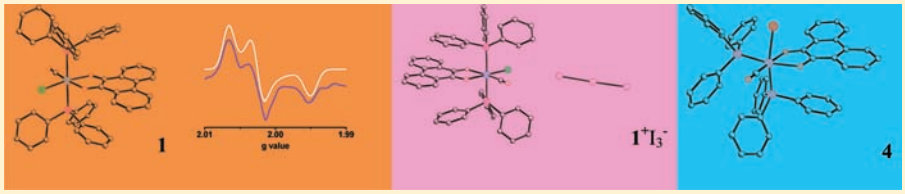

ABSTRACT: The reaction of 9,10-phenanthrenequinone (PQ) with $[M^{II}(H)(CO)(X)(PPh_3)_3]$ in boiling toluene leads to the homolytic cleavage of the M^{II}–H bond, affording the paramagnetic *trans*-$[M(PQ)(PPh_3)_2(CO)X]$ (M = Ru, X = Cl, **1**; M = Os, X = Br, **3**) and *cis*-$[M(PQ)(PPh_3)_2(CO)X]$ (M = Ru, X = Cl, **2**; M = Os, X = Br, **4**) complexes. Single-crystal X-ray structure determinations of **1**, **2**·toluene, and **4**·CH_2Cl_2, EPR spectra, and density functional theory (DFT) calculations have substantiated that **1**–**4** are 9,10-phenanthrenesemiquinone radical ($PQ^{\bullet-}$) complexes of ruthenium(II) and osmium(II) and are defined as *trans*-$[Ru^{II}(PQ^{\bullet-})(PPh_3)_2(CO)Cl]$ (**1**), *cis*-$[Ru^{II}(PQ^{\bullet-})(PPh_3)_2(CO)Cl]$ (**2**), *trans*-$[Os^{II}(PQ^{\bullet-})(PPh_3)_2(CO)\ Br]$ (**3**), and *cis*-$[Os^{II}(PQ^{\bullet-})(PPh_3)_2(CO)Br]$ (**4**). Two comparatively longer C–O [average lengths: **1**, 1.291(3) Å; **2**·toluene, 1.281(5) Å; **4**·CH_2Cl_2, 1.300(8) Å] and shorter C–C lengths [**1**, 1.418(5) Å; **2**·toluene, 1.439(6) Å; **4**·CH_2Cl_2, 1.434(9) Å] of the OO chelates are consistent with the presence of a reduced $PQ^{\bullet-}$ ligand in **1**–**4**. A minor contribution of the alternate resonance form, *trans*- or *cis*-$[M^{I}(PQ)(PPh_3)_2(CO)X]$, of **1**–**4** has been predicted by the anisotropic X- and Q-band electron paramagnetic resonance spectra of the frozen glasses of the complexes at 25 K and unrestricted DFT calculations on **1**, *trans*-$[Ru(PQ)(PMe_3)_2(CO)Cl]$ (**5**), *cis*-$[Ru(PQ)(PMe_3)_2(CO)Cl]$ (**6**), and *cis*-$[Os(PQ)(PMe_3)_2(CO)Br]$ (**7**). However, no thermodynamic equilibria between $[M^{II}(PQ^{\bullet-})(PPh_3)_2(CO)X]$ and $[M^{I}(PQ)(PPh_3)_2(CO)X]$ tautomers have been detected. **1**–**4** undergo one-electron oxidation at −0.06, −0.05, 0.03, and −0.03 V versus a ferrocenium/ferrocene, Fc^+/Fc, couple because of the formation of PQ complexes as *trans*-$[Ru^{II}(PQ)(PPh_3)_2(CO)Cl]^+$ (1^+), *cis*-$[Ru^{II}(PQ)(PPh_3)_2(CO)Cl]^+$ (2^+), *trans*-$[Os^{II}(PQ)(PPh_3)_2(CO)Br]^+$ (3^+), and *cis*-$[Os^{II}(PQ)(PPh_3)_2(CO)Br]^+$ (4^+). The trans isomers **1** and **3** also undergo one-electron reduction at −1.11 and −0.96 V, forming PQ^{2-} complexes *trans*-$[Ru^{II}(PQ^{2-})(PPh_3)_2(CO)Cl]^-$ (1^-) and *trans*-$[Os^{II}(PQ^{2-})(PPh_3)_2(CO)Br]^-$ (3^-). Oxidation of **1** by I_2 affords diamagnetic $1^+I_3^-$ in low yields. Bond parameters of $1^+I_3^-$ [C–O, 1.256(3) and 1.258(3) Å; C–C, 1.482(3) Å] are consistent with ligand oxidation, yielding a coordinated PQ ligand. Origins of UV–vis/near-IR absorption features of **1**–**4** and the electrogenerated species have been investigated by spectroelectrochemical measurements and time-dependent DFT calculations on **5**, **6**, 5^+, and 5^-.

INTRODUCTION

Stabilization of organic radicals coordinated to transition-metal ions is of topical interest in modern coordination chemistry.[1] A precise definition of the electronic state in such a radical-containing complex is relevant to understanding many natural electron-transfer processes. The key element to model these redox systems is the combination of a redox-active metal ion with a redox-noninnocent ligand that undergoes reduction or oxidation relatively at lower potential, stabilizing in many cases reactive organic radicals, such as benzosemiquinone,[2] iminobenzosemiquinone,[3] diiminobenzosemiquinone,[4] and iminothiobenzosemiquinone,[5] and the more reactive phenoxyl,[6] anilino,[7] aminyl,[8] and thiyl[9] radicals including azo,[10] diimine,[11] and osazone[12] anion radicals. However, the variety of stable radical families in the vast coordination chemistry is still rather limited in scope. Stabilizing new organic or metal-centered radicals[13] and diradicals (either singlet or triplet ground state) in coordination complexes has been an ongoing challenge in chemical research.

Transformations of catecholate or *o*-quinone to *o*-semiquinone radicals coordinated to transition-metal ions have been documented in various biological as well as catalytic aspects.[2,14,15] In this project, we focused on the coordination

Received: February 14, 2012
Published: June 4, 2012

 © 2012 American Chemical Society dx.doi.org/10.1021/ic300327x | *Inorg. Chem.* 2012, 51, 6687–6699

of *o*-quinones to redox-active transition-metal ions to elucidate the electronic state of the complexes. In this particular work, 9,10-phenanthrenequinone (PQ) has been used as a ligand.[16] PQ undergoes facile electron-transfer reactions by biological reducing agents to the 9,10-phenanthrenesemiquinone radical ($PQ^{\bullet -}$). In the presence of intracellular $Fe^{II/III}$, $PQ^{\bullet -}$ transfers the electron to dioxygen molecules, yielding biologically harmful and reactive radical species.[17]

Moreover, the binding of PQ, which is reducible at low potential by one electron, to a redox-active ruthenium or osmium metal ion has been worth investigation in the aspects of valence tautomerization,[18] as shown in Scheme 1.

Scheme 1

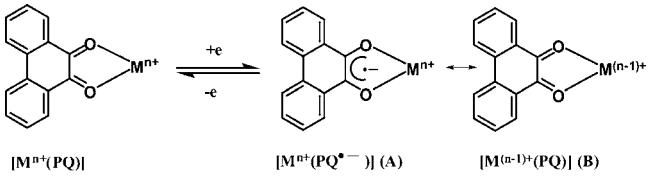

Reportedly, compared to catecholates, unlike other *o*-quinones, PQ is a weaker chelating agent, and a limited number of coordination compounds of it with transition-metal ions has been reported.[19−24] Coordination of PQ to an osmium ion with similar coligands will open up a scope to generalize the discussion of elucidating the electronic structure of the PQ complexes with redox-active metal ions.

In this Article, we report PQ-induced homolytic cleavage of Ru^{II}−H and Os^{II}−H bonds, rendering paramagnetic $[Ru(PQ)(PPh_3)_2(CO)Cl]$ and $[Os(PQ)(PPh_3)_2(CO)Br]$ complexes. Because both the metal (ruthenium and osmium) ions and the PQ ligand are redox-active, $[Ru(PQ)(PPh_3)_2(CO)Cl]$ and $[Os(PQ)(PPh_3)_2(CO)Br]$ complexes can be described by two valence tautomers, as illustrated in Scheme 1. In this work, four geometrical isomers, *trans*-$[Ru(PQ)(PPh_3)_2(CO)Cl]$ (**1**), *cis*-$[Ru(PQ)(PPh_3)_2(CO)Cl]$ (**2**), *trans*-$[Os(PQ)(PPh_3)_2(CO)Br]$ (**3**), and *cis*-$[Os(PQ)(PPh_3)_2(CO)Br]$ (**4**), have been successfully isolated, augmenting a complete experimental and theoretical investigation.

Molecular structures, X- and Q-band electron paramagnetic resonance (EPR) spectra of **1**−**4** (solid, solution, and frozen glass), and density functional theory (DFT) calculations on **1**, *trans*-$[Ru(PQ)(PMe_3)_2(CO)Cl]$ (**5**), *cis*-$[Ru(PQ)(PMe_3)_2(CO)Cl]$ (**6**), and *cis*-$[Os(PQ)(PMe_3)_2(CO)Br]$ (**7**) complexes have established that, although no thermodynamic equilibria of valence tautomers A and B (Scheme 1) in **1**−**4** have been detected, the electronic state of **1**−**4** complexes is best described as a superposition of the tautomers A and B. Ground-state electronic structures of the oxidized and reduced analogues of the complexes have similarly been investigated by isolation and single-crystal X-ray structure determination of an oxidized analogue $\mathbf{1}^+I_3^-$, spectra, cyclic voltammetry, spectroelectrochemical measurements, and time-dependent (TD) DFT calculations on **5**, **6**, $\mathbf{5}^+$, and $\mathbf{5}^-$.

EXPERIMENTAL SECTION

Materials. Reagents or analytical-grade materials were obtained from commercial suppliers and used without further purification. The precursors $[Ru^{II}(H)(CO)(Cl)(PPh_3)_3]$ and $[Os^{II}(H)(CO)(Br)(PPh_3)_3]$ were prepared by reported procedures.[25] All of the physicochemical data were collected on the isolated *trans*-$[Ru(PQ)(PPh_3)_2(CO)Cl]$ (**1**), *cis*-$[Ru(PQ)(PPh_3)_2(CO)Cl]$·toluene (**2**·toluene), *trans*-$[Os(PQ)(PPh_3)_2(CO)Br]$ (**3**), *cis*-$[Os(PQ)(PPh_3)_2(CO)Br]$ (**4**), and *trans*-$[Ru(PQ)(PPh_3)_2(CO)Cl]^+I_3^-$ ($\mathbf{1}^+I_3^-$) complexes.

Syntheses. *trans-[Ru(PQ)(PPh$_3$)$_2$(CO)Cl] (**1**).* To PQ (40 mg, 0.2 mmol) in toluene (30 mL) was added $[Ru^{II}(H)(CO)(Cl)(PPh_3)_3]$ (200 mg, 0.2 mmol). The mixture was refluxed for 40 min under argon and allowed to cool at room temperature (298 K). Dark-brown microcrystals of **1** separated out and then were filtered and dried in air. Yield: 80 mg (40% with respect to ruthenium). For single-crystal X-ray structure determination and all spectroscopic and electrochemical measurements, the product was further recrystallized by diffusing *n*-hexane to the CH_2Cl_2 solution of the crude product at room temperature. Mass spectral data [electrospray ionization (ESI), positive ion, CH_2Cl_2]: *m*/*z* 862.0 for [**1**-Cl]$^+$. Anal. Calcd for $C_{51}H_{38}ClO_3P_2Ru$: C, 68.27; H, 4.27. Found: C, 68.02; H, 4.19. IR/cm^{-1} (KBr): ν 1950 (vs, $\nu_{C\equiv O}$), 1595 (s, $\nu_{C=C(PQ)}$), 1458 (s, $\nu_{C=O(sym)}$), 1432 (s, $\nu_{C=O(asym)}$), 1203 (m, $\nu_{C-H(bend)}$), 1092 (m, $\nu_{PQ(skel)}$), 756 (m, $\nu_{C-H(wagg)}$), 693 (s, $\nu_{Ru-P(sym)}$), 521 (s, $\nu_{Ru-P(asym)}$).

*cis-[Ru(PQ)(PPh$_3$)$_2$(CO)Cl]·Toluene (**2**·Toluene).* The filtrate of the above reaction was allowed to evaporate slowly under air at room temperature (298 K). After 4−5 days, dark-brown single crystals of **2**·toluene separated out and then were filtered and dried in air. Yield: 100 mg (50% with respect to ruthenium). Single crystals for the X-ray diffraction study were collected from this product. Mass spectral data (ESI, positive ion, CH_2Cl_2): *m*/*z* 862.0 for [**2**-Cl]$^+$. Anal. Calcd for $C_{58}H_{46}ClO_3P_2Ru$: C, 70.40; H, 4.69. Found: C, 70.23; H, 4.58. IR/cm^{-1} (KBr): ν 1950 (vs, $\nu_{C\equiv O}$), 1594 (s, $\nu_{C=C(PQ)}$), 1458 (s, $\nu_{C=O(sym)}$), 1433 (s, $\nu_{C=O(asym)}$), 1203 (m, $\nu_{C-H(bend)}$), 1092 (m, $\nu_{PQ(skel)}$), 756 (m, $\nu_{C-H(wagg)}$), 693 (s, $\nu_{Ru-P(sym)}$), 521 (s, $\nu_{Ru-P(asym)}$).

*trans-[Os(PQ)(PPh$_3$)$_2$(CO)Br] (**3**).* To PQ (40 mg, 0.2 mmol) in toluene (30 mL) was added $[Os^{II}(H)(CO)(Br)(PPh_3)_3]$ (220 mg, 0.2 mmol). The mixture was refluxed for 40 min under argon and allowed to cool at room temperature (298 K). A few dark-brown microcrystals of **3** separated out and then were filtered and dried in air. Yield: 12 mg (6% with respect to osmium). The product was used for all spectroscopic and electrochemical measurements. Mass spectral data (ESI, positive ion, CH_2Cl_2): *m*/*z* 952.0 for [**3**-Br]$^+$. Anal. Calcd for $C_{51}H_{38}BrO_3P_2Os$: C, 59.42; H, 3.72. Found: C, 59.12; H, 3.70. IR/cm^{-1} (KBr): ν 1909 (vs, $\nu_{C\equiv O}$), 1654 (s, $\nu_{C=C(PQ)}$), 1482 (s, $\nu_{C=O(sym)}$), 1434 (s, $\nu_{C=O(asym)}$), 1203 (m, $\nu_{C-H(bend)}$), 1096 (m, $\nu_{PQ(skel)}$), 756 (m, $\nu_{C-H(wagg)}$), 692 (s, $\nu_{Ru-P(sym)}$), 520 (s, $\nu_{Ru-P(asym)}$).

*cis-[Os(PQ)(PPh$_3$)$_2$(CO)Br] (**4**).* The filtrate of the above reaction was allowed to evaporate slowly under air at room temperature (298 K). After 4−5 days, dark-brown single crystals of **4** separated out and then were filtered and dried in air. Yield: 100 mg (50% with respect to osmium). Single crystals of **4**·CH_2Cl_2 for X-ray diffraction were grown by diffusion of *n*-hexane to the CH_2Cl_2 solution of **4**. Mass spectral data (ESI, positive ion, CH_2Cl_2): *m*/*z* 952.0 for [**4**-Br]$^+$. Anal. Calcd for $C_{51}H_{38}BrO_3P_2Os$: C, 59.42; H, 3.72. Found: C, 59.08; H, 3.57. IR/cm^{-1} (KBr): ν 1932 (vs, $\nu_{C\equiv O}$), 1653 (s, $\nu_{C=C(PQ)}$), 1458 (s, $\nu_{C=O(sym)}$), 1433 (s, $\nu_{C=O(asym)}$), 1092 (m, $\nu_{PQ(skel)}$), 755 (m, $\nu_{C-H(wagg)}$), 695 (s, $\nu_{Ru-P(sym)}$), 524 (s, $\nu_{Ru-P(asym)}$).

trans-[Ru(PQ)(PPh$_3$)$_2$(CO)Cl]I$_3$ ($\mathbf{1}^+I_3^-$). To a solution of **1** (100 mg, 0.1 mmol) in CH_2Cl_2 (20 mL) was added a I_2 (25 mg, 0.1 mmol) solution in *n*-hexane (20 mL), and it was allowed to diffuse at 298 K. After 4−5 days, black needles of $\mathbf{1}^+I_3^-$ separated out and then were filtered and dried in air (single crystals for X-ray diffraction have been collected from these products). Yield: 5 mg (5% with respect to **1**). Mass (ESI, positive ion, CH_2Cl_2): *m*/*z* 898.3 for [**1**]$^+$. Anal. Calcd for $C_{51}H_{38}ClO_3P_2RuI_3$: C, 47.93; H, 2.99. Found: C, 47.78; H, 2.93. ^{1}H NMR ($CDCl_3$, 600 MHz): δ 8.21 (d, 2H), 9.03 (d, 2H), 7.73 (t, 2H), 7.66 (m, 4H), 7.54 (m, 4H), 7.46 (m, 8H), 7.37 (m, 4H), 7.31 (m, 8H), 7.19 (m, 4H). IR/cm^{-1} (KBr): ν 1980 (vs, $\nu_{C\equiv O}$), 1654 (s, $\nu_{C=O(sym)}$), 1597 (s, $\nu_{C=C(PQ)}$), 1560 (s, $\nu_{C=O(asym)}$), 1436, 1364, 1095 (m, $\nu_{PQ(skel)}$), 747 (m, $\nu_{C-H(wagg)}$), 694 (s, $\nu_{Ru-P(sym)}$), 518 (s, $\nu_{Ru-P(asym)}$).

Physical Measurements. Commercially available spectroscopic-grade solvents were used for spectroscopic and electrochemical measurements. The carbon and hydrogen contents of the compounds were obtained from a Perkin-Elmer 2400 series II elemental analyzer.

dx.doi.org/10.1021/ic300327x | *Inorg. Chem.* 2012, 51, 6687−6699

Table 1. Crystallographic Data for 1, $1^+I_3^-$, 2·Toluene, and $4\cdot CH_2Cl_2$

	1	$1^+I_3^-$	2·toluene	$4\cdot CH_2Cl_2$
formula	$C_{51}H_{38}ClO_3P_2Ru$	$C_{51}H_{38}ClO_3P_2RuI_3$	$C_{58}H_{46}ClO_3P_2Ru$	$C_{52}H_{40}BrCl_2O_3P_2Os$
fw	897.27	1277.97	989.41	1115.79
cryst color	dark brown	dark brown	dark brown	dark brown
cryst syst	orthorhombic	monoclinic	monoclinic	monoclinic
space group	*Pbcn*	$P2_1/c$	$P2_1/n$	$P2_1/n$
a (Å)	20.4786(19)	13.2074(3)	10.4539(3)	10.305(2)
b (Å)	11.5413(11)	14.1428(3)	29.3592(8)	28.966(6)
c (Å)	17.5033(15)	25.2055(5)	15.5500(4)	15.146(3)
β (deg)		90.265(1)	90.107(2)	90.189(3)
V (Å^3)	4136.9(7)	4708.08(17)	4772.6(2)	4520.9(15)
Z	4	4	4	4
T (K)	296(2)	100(2)	296(2)	100(2)
calcd (g cm^{-3})	1.441	1.803	1.377	1.639
reflns collected	29511	78295	62701	22679
unique reflns	3642	10998	8415	7936
refection $[I > 2\sigma(I)]$	3336	10152	6825	6778
λ (Å)/μ (mm^{-1})	0.71073/0.565	0.71073/2.467	0.71073/0.497	0.71073/3.937
F(000)	1836	2472	2036	2204
R1[a] $[I > 2\sigma(I))]$/ GOF[b]	0.0293/0.926	0.0237/1.064	0.0528/1.220	0.0469/1.153
R1[a] (all data)	0.0327	0.0267	0.0703	0.0570
wR2[c] $[I > 2\sigma(I)]$	0.0757	0.0532	0.1133	0.1157
no. of param	264	550	583	568
residual density (e Å^{-3})	0.455	1.429	0.716	3.067

[a] $R1 = \sum||F_o| - |F_c||/\sum|F_o|$. [b] $GOF = \{\sum[w(F_o^2 - F_c^2)^2]/(n-p)\}^{1/2}$, [c] $wR2 = [\sum[w(F_o^2 - F_c^2)^2]/\sum[w(F_o^2)^2]]^{1/2}$, where $w = 1/[\sigma^2(F_o^2) + (aP)^2 + bP]$, $P = (F_o^2 + 2F_c^2)/3$.

IR spectra of the samples were measured from 4000 to 400 cm^{-1} with KBr pellets at room temperature on a Perkin-Elmer Spectrum RX I Fourier transform IR spectrophotometer. ^{1}H NMR spectra in a $CDCl_3$ solvent were carried out on a Bruker Avance DPX-600 MHz spectrometer. ESI mass spectra were recorded on a micromass Q-TOF mass spectrometer. Electronic absorption spectra in solution at 298 K were carried out on a Perkin-Elmer Lambda 25 spectrophotometer in the range of 1100−200 nm. The X-band EPR spectra were measured on a Bruker EMX spectrometer, where the microwave frequency was measured with a Hewlett-Packard 5246 L electronic counter. Q-band spectra were measured using a Bruker EMX spectrometer with microwave frequency = 33.936 GHz, power = 1.997 mW, and modulation amplitude = 2.00 G. The magnetic susceptibility at 298 K was measured on a Sherwood magnetic susceptibility balance. The electroanalytical instrument BASi Epsilon-EC for cyclic voltammetry experiments in a CH_2Cl_2 solution containing 0.2 M tetrabutylammonium hexafluorophosphate as the supporting electrolyte was used. The BASi platinum working electrode, platinum auxiliary electrode, and Ag/AgCl reference electrode were used for the measurements. The redox potential data are referenced versus a ferrocenium/ferrocene, Fc^+/Fc, couple. In all cases, the experiments were performed with multiple scan rates to analyze the reversibility of the electron-transfer waves. A BASi SEC-C thin-layer quartz glass spectroelectrochemical cell kit (light path length of 1 mm) with a platinum gauze working electrode and a SEC-C platinum counter electrode was used for spectroelectrochemistry measurements.

X-ray Crystallographic Data Collection and Refinement of the Structures. Dark-brown single crystals of **1**, **2**·toluene, $\mathbf{4}\cdot CH_2Cl_2$, and $\mathbf{1}^+I_3^-$ were picked up with a nylon loop, which was mounted on a Bruker Kappa CCD diffractometer equipped with a molybdenum target rotating-anode X-ray source and a graphite monochromator (Mo Kα, λ = 0.71073 Å). Final cell constants were obtained from least-squares fits of all measured reflections. Structures were readily solved by the Patterson method and subsequent difference Fourier techniques. The crystallographic data are listed in Table 1. *SHELX97*[26] was used for the structure solution and refinement. All non-hydrogen atoms were refined anisotropically. Hydrogen atoms were placed at calculated positions and refined as riding atoms with isotropic displacement parameters. The carbon monoxide (CO) and chloride ligands are disordered with respect to the coordinated PQ plane and have been refined with 50% occupancies in both positions of each atom in **1**. The solvent molecules in **2**·toluene and $\mathbf{4}\cdot CH_2Cl_2$ are heavily disordered, and in the case of **2**·toluene, it is refined isotropically.

DFT Calculations. All calculations reported in this Article were done with the *Gaussian 03W*[27] program package supported by *GaussView 4.1*. The DFT[28] and TD DFT[29] calculations were performed at the level of the Becke three-parameter hybrid functional with the nonlocal correlation functional of Lee−Yang−Parr (B3LYP).[30] Gas-phase geometries of **1** and **5**−**7** with a doublet spin state were optimized using Pulay's Direct Inversion[31] in the Iterative Subspace (DIIS), "tight" convergent self-consistent-field procedure[32] ignoring symmetry. Similarly, gas-phase geometries of *trans*-$[Ru(PQ)(PMe_3)_2(CO)Cl]^+$ ($\mathbf{5}^+$), *trans*-$[Ru(PQ)(PMe_3)_2(CO)Cl]^-$ ($\mathbf{5}^-$), and $Ru(CO)_3$ (chrysenequinone) were optimized with a singlet spin state. Frequencies of molecular (bond) vibrations were calculated on **5**. In all calculations, a LANL2DZ basis set along with the corresponding effective core potential was used for ruthenium and osmium metals.[33−35] A valence double-ζ basis set, 6-31G,[36] was used for hydrogen atoms. For carbon, oxygen, phosphorus, chlorine, and non-hydrogen atoms, a valence double-ζ basis set with diffuse and polarization functions, 6-31++G**,[37] was employed for all calculations. The percentage contributions of metal, chloride, and PQ ligands to the frontier orbitals were calculated using the *GaussSum* program package.[38] The 60 lowest singlet-excitation energies on each of the optimized geometries of **5**, **6**, $\mathbf{5}^+$, and $\mathbf{5}^-$ were calculated by the TD DFT method.[39] The nature of transitions was calculated by adding the probability of the same type among α and β molecular orbitals.

RESULTS AND DISCUSSION

Syntheses and Characterization. The paramagnetic and diamagnetic PQ complexes of ruthenium and osmium isolated in this work are listed in Chart 1. The dark-brown paramagnetic complexes **1** and **2**·toluene were isolated in moderate yield

dx.doi.org/10.1021/ic300327x | *Inorg. Chem.* 2012, 51, 6687−6699

Chart 1. Isolated PQ Complexes of Ruthenium and Osmium (Cis and Trans Isomers with Respect to PPh_3 Ligands)

trans-[Ru(PQ)$(PPh_3)_2$(CO)Cl]	$S = {}^1/_2$	**1**
cis-[Ru(PQ)$(PPh_3)_2$(CO)Cl]·(toluene)	$S = {}^1/_2$	**2**·(toluene)

from the reaction of a ruthenium hydride precursor, $[Ru^{II}(H)(CO)(Cl)(PPh_3)_3]$, with PQ in boiling toluene. Homolytic cleavage of the Ru^{II}–H bond affords one-electron paramagnetic **1** and **2**·toluene (eq 1). **3** and **4** were synthesized by a similar reaction of $[Os^{II}(H)(CO)(Br)(PPh_3)_3]$ with PQ in boiling toluene (eq 2). The yield of **3** is comparatively low (~6%). Diffusion of I_2 in *n*-hexane to the CH_2Cl_2 solution of **1** generates $\mathbf{1}^+I_3^-$ in low yield. The $\nu_{C\equiv O}$ value in **1** and **2**·toluene appears at 1950 cm^{-1}, while in $\mathbf{1}^+I_3^-$, it resonates at comparatively higher frequency, 1980 cm^{-1} (Figure S1, Supporting Information). In **3** and **4** incorporating 5d metal ions, $\nu_{C\equiv O}$ appears respectively at 1909 and 1932 cm^{-1}. The symmetric and antisymmetric $\nu_{C=O}$ values of the PQ ligand in **1**–**4** complexes are significant to analyze the electronic state of the PQ ligand. In $PQ^{\bullet-}$ complexes **1**–**4**, they appear at 1480–1430 cm^{-1}, while in $\mathbf{1}^+I_3^-$, it appears at 1654 and 1560 cm^{-1}, correlating the neutral PQ chelate. The frequencies of molecular bond vibrations were calculated on **5** at the B3LYP/DFT level of theory, and the results have been used to assign the IR spectra of **1**–**4** and $\mathbf{1}^+I_3^-$ complexes. Data are listed in the Experimental Section. Single-crystal X-ray structure determinations have confirmed the molecular geometries of **1**, $\mathbf{1}^+I_3^-$, **2**·toluene, and **4**, while the geometry of **3** has been assigned by the UV–vis/near-IR (NIR) spectrum and electrochemical properties.

$$[Ru^{II}(PPh_3)_3(CO)(H)Cl] + PQ(\text{toluene solution}) \rightarrow \mathbf{1} + \mathbf{2}\cdot\text{toluene} + \frac{1}{2}H_2 + PPh_3 \quad (1)$$

$$[Os^{II}(PPh_3)_3(CO)(H)Br] + PQ(\text{toluene solution}) \rightarrow \mathbf{3}(\text{minor}) + \mathbf{4} + \frac{1}{2}H_2 + PPh_3 \quad (2)$$

The UV–vis/NIR spectra of **1**–**4** and $\mathbf{1}^+I_3^-$ are shown in Figures 1 and 2, and the spectral data are summarized in Table 2. The electronic absorption spectra of **2**·toluene and **4** are similar, signaturing the characteristic absorption features of cis geometry (see the Electronic Absorption Spectra section). The

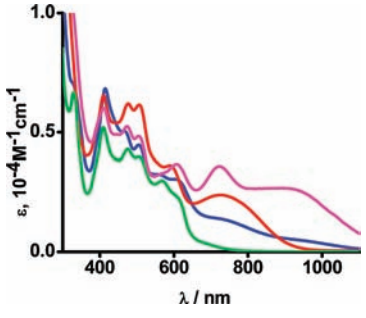

Figure 1. UV–vis/NIR spectra of **1** (red), **2** (green), **3** (pink), and **4** (blue).

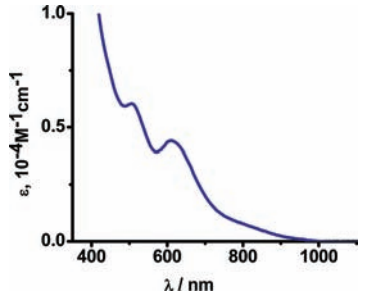

Figure 2. UV–vis/NIR spectrum of $\mathbf{1}^+I_3^-$ in CH_2Cl_2.

Table 2. Electronic Spectra of 1–4 and $\mathbf{1}^+I_3^-$ Complexes in CH_2Cl_2 at 298 K

complexes	λ_{max}/nm ($\varepsilon/10^4$ M^{-1} cm^{-1})
1	735(0.25), 588(0.36), 506(0.63), 475(0.64), 410(0.66)
$\mathbf{1}^+I_3^-$	820(0.07), 610(0.44), 505(0.60)
2	612(0.23), 567(0.29), 508(0.41), 475(0.43), 408(0.53), 329(0.67)
3	940(0.26), 724(0.36), 608(0.37), 506(0.48), 471(0.52), 410(0.60)
4	611(0.30), 557(0.33), 505(0.45), 468(0.50), 412(0.68), 331(0.70)

electronic spectra of the trans analogues **1** and **3** with a low-energy absorption band at 734 nm are different from those of **2**·toluene and **4** (Figure 1). The absorption band at around 410 nm and a moderately weaker band at 600 nm are characteristic for all of these complexes. The low-energy absorption maxima of **1** at 588 and 735 nm are red-shifted to 610 and 820 nm in $\mathbf{1}^+I_3^-$ (Table 2 and Figure 2). The change of absorption features upon reduction of **1** to $\mathbf{1}^-$ was recorded by a spectroelectrochemistry measurement (vide infra). The origins of the absorptions of **1**–**4**, their oxidized and reduced analogues, were investigated by TD DFT calculations on **5** and **6** isomers and $\mathbf{5}^+$ and $\mathbf{5}^-$ ions. The calculated results have been included in the Electronic Absorption Spectra section.

X-ray Structures. **1** crystallizes in the space group *Pbcn*, considering CO and chloride ligands crystallographically disordered. The structure was refined with an occupancy of 0.5 for each of chlorine atoms and CO molecules for one of the octahedral sites. Further, the chlorine and oxygen atoms of the CO molecule appear to be disordered with respect to the plane containing the PQ ligand. An ORTEP plot of **1** with an atom-labeling scheme is shown in Figure 3, displaying one of the disordered positions of the chloride and CO ligands. The significant bond parameters are summarized in Table 3.

Bond angles have revealed the distorted octahedral coordination sphere around the ruthenium center, particularly the chelate bite of the quinone ligand being 78.5°. The bond parameters do not support the diketo structure of the PQ ligand in **1**. Expected C–O and C–C lengths are 1.24 and 1.45 Å for the neutral quinone structure of a PQ ligand.[19–24] In **1**, the C–C length, 1.418 (5) Å, of the chelate is shorter than a $C(sp^2)$–$C(sp^2)$ single bond, while the C–O length, 1.291(3) Å, is comparatively longer than a C=O double bond. This trend of C–C and C–O lengths of the chelate in **1** suggests the presence of a reduced 9,10-phenanthrenesemiquinone radical ($PQ^{\bullet-}$) ligand, and compound **1** is defined as a $PQ^{\bullet-}$ complex of ruthenium(II) as tautomer A in Scheme 1.

The similar bond-length trend of the OO chelate has been established in other 9,10-phenanthrenesemiquinone radicals

dx.doi.org/10.1021/ic300327x | *Inorg. Chem.* 2012, 51, 6687–6699

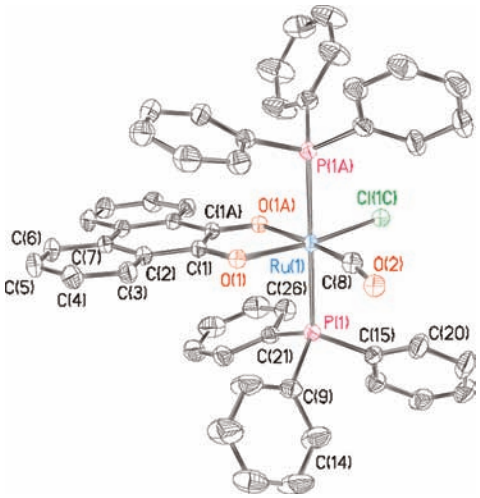

Figure 3. ORTEP plot of **1** with 40% thermal ellipsoids (hydrogen atoms are omitted for clarity).

reported by Tuck et al. and Pierpont et al.:[19] benzosemiquinonates[2,14,15] and one-electron-reduced 1,2-diketo anion-radical species.[40] The Ru^{II}–PPh_3, Ru^{II}–Cl, and Ru^{II}–CO distances correlate well with those reported in other *trans*-$Ru^{II}(PPh_3)_2$ species incorporating CO and chloride as coligands.[10,12,3e]

2·toluene crystallizes in space group $P2_1/n$. Two bulky PPh_3 ligands in **2**·toluene are cis to each other. A molecular view and an atom-labeling scheme of **2**·toluene are depicted in Figure 4. Selected bond parameters are summarized in Table 4. Similar to those in **1**, the C–O bond lengths of the OO chelate are comparatively longer and the C–C length is shorter, correlating well with the 9,10-phenanthrenesemiquinone radical description, and **2** is described as the $PQ^{\bullet-}$ complex of ruthenium(II). Because of stronger $Ru^{II} \rightarrow PPh_3$ π-back-bonding in *cis*-$Ru^{II}(PPh_3)_2$ geometry, the Ru^{II}–PPh_3 bonds in **2** are relatively shorter than those in **1**, with *trans*-$Ru^{II}(PPh_3)_2$ geometry. The effect of stronger $Ru^{II} \rightarrow PPh_3$ π-back-bonding is also reflected in the Ru–Cl bond trans to a PPh_3 ligand. The trend is as follows: Ru^{II}–Cl in **2**·toluene > Ru^{II}–Cl in **1**.

4·CH_2Cl_2 crystallizes in space group $P2_1/n$. The molecular geometry and atom-labeling scheme are illustrated in Figure 5. Table 5 summarizes the selected bond parameters. The bond parameters of the OO chelate are comparable to those in **1** and **2**·toluene, prompting the coordination of $PQ^{\bullet-}$ to the Os^{II} ion. Two Os^{II}–PPh_3 and two Os^{II}–O lengths are comparable to those in the cis isomer **2**·toluene. DFT calculations on *trans*-[Os(PQ)$(PMe_3)_2$(CO)Br] (**7**) have revealed the analogous bond parameters and spin-density localization on the PQ chelate, inferring that tautomer A provides the larger contribution to the electronic structure of **4**.

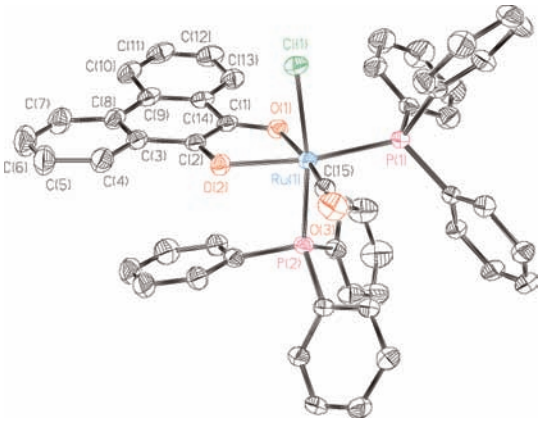

Figure 4. ORTEP plot of **2**·toluene with 40% thermal ellipsoids (the toluene molecule and hydrogen atoms are omitted for clarity).

Table 4. Selected Experimental Bond Lengths (Å) and Angles (deg) of 2·Toluene and Corresponding Calculated Parameters of 6

	exptl (**2**·toluene)	calcd (**6**)		exptl (**2**·toluene)	calcd (**6**)
Ru(1)–O(1)	2.106 (3)	2.158	O(1)–Ru(1)–O(2)	77.8(3)	77.00
Ru(1)–O(2)	2.117(3)	2.151	O(1)–C(1)–C(2)	118.5(4)	118.70
Ru(1)–P(1)	2.327(3)	2.352	O(2)–C(2)–C(1)	118.0(4)	118.93
Ru(1)–P(2)	2.372(3)	2.348	C(1)–O(1)–Ru(1)	112.7(3)	111.79
Ru(1)–Cl(1)	2.420(3)	2.496	C(2)–O(2)–Ru(1)	112.5(3)	112.09
Ru(1)–C(15)	1.823(5)	1.863	C(15)–Ru(1)–Cl(1)	92.1(3)	91.41
O(1)–C(1)	1.281(6)	1.293	Cl(1)–Ru(1)–O(1)	85.0(2)	87.13
O(2)–C(2)	1.282(5)	1.288	Cl(1)–Ru(1)–O(2)	83.6(2)	86.17
C(1)–C(2)	1.439(6)	1.438	P(1)–Ru(1)–P(2)	99.9(1)	100.52

1$^+I_3^-$ crystallizes in space group $P2_1/c$. The molecular geometry and atom-labeling scheme are shown in Figure 6. Table 6 summarizes the selected bond parameters. The X-ray structure authenticates the trans geometries and molecular compositions of **1**$^+I_3^-$ and **1**. The bond parameters of the OO chelate of **1**$^+I_3^-$ are different from those in **1**, **2**·toluene, and **4**·CH_2Cl_2. Relatively shorter C–O, 1.256(3) and 1.258(3) Å, and longer C(1)–C(2), 1.482(3) Å, lengths are consistent with the neutral PQ chelation defining the complex as a coordination compound of PQ of ruthenium(II) as in *trans*-

Table 3. Selected Experimental Bond Lengths (Å) and Angles (deg) of 1 and Corresponding Calculated Parameters of 1 and 5

		calcd				calcd	
	exptl (**1**)	**1**	**5**		exptl (**1**)	**1**	**5**)
Ru(1)–O(1)	2.088(2)	2.175	2.183	O(1)–C(1)	1.291(3)	1.290	1.292
Ru(1)–O(1A)	2.088(2)	2.124	2.115	C(1)–C(1A)	1.418(5)	1.433	1.434
Ru(1)–P(1)	2.396(4)	2.471	2.416	O(1)–Ru(1)–O(1A)	78.5(2)	76.38	76.88
Ru(1)–P(1A)	2.396(4)	2.470	2.416	O(1)–C(1)–C(1A)	118.3(3)	118.27	118.61
Ru(1)–Cl(1)	2.344(8)	2.449	2.466	C(1)–O(1)–Ru(1)	112.4(3)	112.75	111.87
Ru(1)–C(8)	1.841(8)	1.854	1.851	C(8)–Ru(1)–Cl(1)	95.8(4)	94.76	92.61
O(1A)–C(1A)	1.291(3)	1.296	1.295	Cl(1)–Ru(1)–O(1)	91.6(3)	92.57	94.76

dx.doi.org/10.1021/ic300327x | *Inorg. Chem.* 2012, 51, 6687–6699

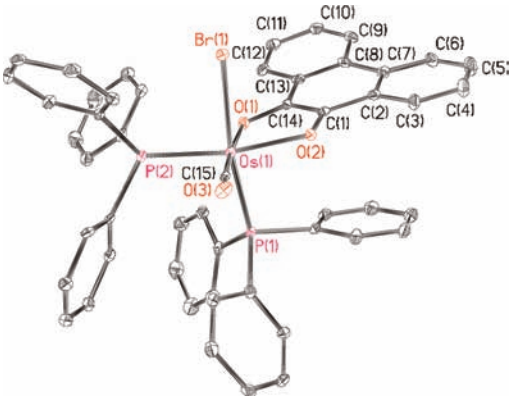

Figure 5. ORTEP plot of $4{\cdot}CH_2Cl_2$ with 40% thermal ellipsoids (CH_2Cl_2 and hydrogen atoms are omitted for clarity).

Table 5. Selected Experimental Bond Lengths (Å) and Angles (deg) of $4{\cdot}CH_2Cl_2$ and Corresponding Calculated Parameters of 7

	exptl ($4{\cdot}CH_2Cl_2$)	calcd (7)		exptl ($4{\cdot}CH_2Cl_2$)	calcd (7)
Os(1)–O(1)	2.091(5)	2.145	O(1)–Os(1)–O(2)	77.26(16)	76.18
Os(1)–O(2)	2.133(4)	2.162	O(1)–C(1)–C(2)	116.8(6)	118.32
Os(1)–P(1)	2.357(2)	2.342	O(2)–C(2)–C(1)	118.2(5)	118.12
Os(1)–P(2)	2.324(2)	2.349	C(1)–O(1)–Os(1)	113.9(4)	113.54
Os(1)–C(15)	1.832(7)	1.858	C(2)–O(2)–Os(1)	113.0(4)	112.95
Os(1)–Br(1)	2.556(2)	2.635	C(15)–Os(1)–Br(1)	92.81(18)	92.98
O(1)–C(1)	1.315(7)	1.292	Br(1)–Os(1)–O(1)	84.09(11)	84.46
O(2)–C(2)	1.286(8)	1.296	Br(1)–Os(1)–O(2)	82.24(11)	85.66
C(1)–C(2)	1.434(9)	1.433	P(1)–Os(1)–P(2)	99.29(6)	100.31

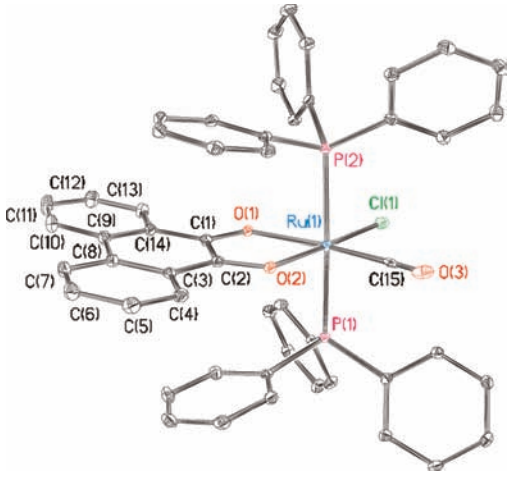

Figure 6. ORTEP plot of $1^+I_3^-$ with 40% thermal ellipsoids (I_3^- ion and hydrogen atoms are omitted for clarity).

Table 6. Selected Experimental Bond Lengths (Å) and Angles (deg) of $1^+I_3^-$ and Corresponding Calculated Parameters of 5^+

	exptl ($1^+I_3^-$)	calcd (5^+)		exptl ($1^+I_3^-$)	calcd (5^+)
Ru(1)–O(1)	2.1494(15)	2.211	O(1)–Ru(1)–O(2)	76.11(6)	73.87
Ru(1)–O(2)	2.0401(15)	2.094	O(1)–C(1)–C(2)	116.00(19)	115.95
Ru(1)–P(1)	2.3891(5)	2.449	O(2)–C(2)–C(1)	116.00(19)	115.73
Ru(1)–P(2)	2.3946(5)	2.449	C(1)–O(1)–Ru(1)	114.06(13)	115.18
Ru(1)–Cl(1)	2.3977(6)	2.421	C(2)–O(2)–Ru(1)	117.79(14)	119.27
Ru(1)–C(15)	1.917(3)	1.854	C(15)–Ru(1)–Cl(1)	94.12(7)	92.88
O(1)–C(1)	1.256(3)	1.256	Cl(1)–Ru(1)–O(1)	99.18(4)	96.75
O(2)–C(2)	1.258(3)	1.261	Cl(1)–Ru(1)–O(2)	175.08(4)	170.62
C(1)–C(2)	1.482(3)	1.492	P(1)–Ru(1)–P(2)	175.90(2)	168.27

$[Ru^{II}(PPh_3)(PQ)(CO)(Cl)]^+I_3^-$. The trend of bond parameters of the PQ chelate of $1^+I_3^-$ is similar to those found in the $Cu^{I}PQ$ complex, $[Cu(dppf)(PQ)]BF_4$ [average of the C–O lengths: 1.250(11) Å; C–C length, 1.499(13) Å], reported by Kaim et al.[21]

EPR Spectra. Magnetic susceptibility measurements at 298 K confirmed the one-electron paramagnetism of **1**–**4** (μ_{eff} = 1.75–1.81 μ_B). X-band EPR spectra of solids (298 K), solutions (298 K), and frozen CH_2Cl_2 glasses (25 K) of **1**–**4** were recorded. Q-band EPR spectra of frozen glasses of **1** and **2** at 25 K were also recorded. All of the spectra are illustrated in Figures 7–9, and the EPR parameters are summarized in Table 7. It is to be noted that the EPR spectra of solids at 298 K and frozen glasses at 25 K of **1**–**4** are anisotropic because of a minor contribution of the resonance form B (Scheme 1) incorporating ruthenium(I) or osmium(I) coordinated to π-acidic PQ. The isotropic fluid solution EPR spectrum of the *trans* isomer **1** has been simulated well considering $^{35,37}Cl$

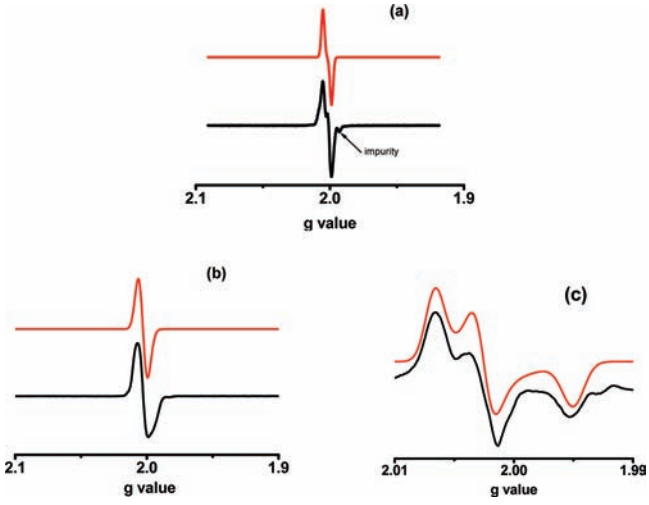

Figure 7. (a) X-band EPR spectra in a CH_2Cl_2 solution at 298 K showing $^{35,37}Cl$ hyperfine coupling. The satellite appears due to an impurity. (b) X- and (c) Q-band EPR spectra of frozen glasses at 25 K of **1** (black = experimental spectra; red = simulated spectra).

dx.doi.org/10.1021/ic300327x | Inorg. Chem. 2012, 51, 6687–6699

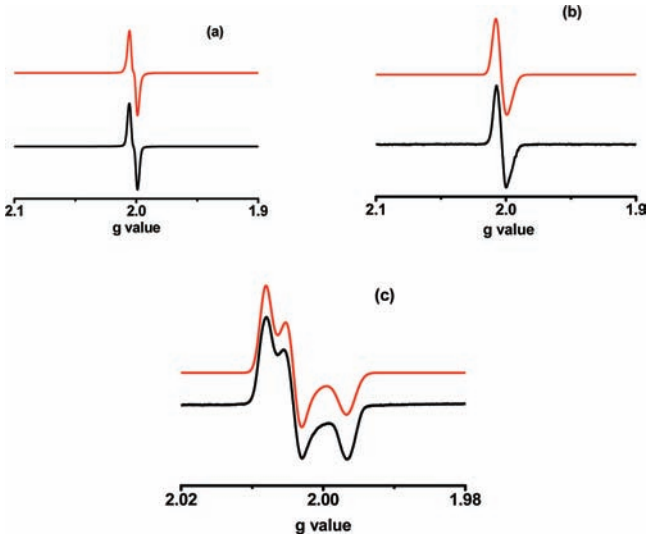

Figure 8. (a) X-band EPR spectra in a CH_2Cl_2 solution at 298 K showing hyperfine coupling due to one of the PPh_3 ligands. (b) X- and (c) Q-band EPR spectra of frozen CH_2Cl_2 glasses at 25 K of **2** (black = experimental spectra; red = simulated spectra).

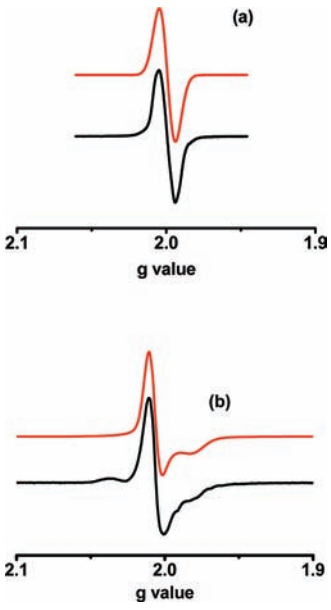

Figure 9. X-band EPR spectra of (a) CH_2Cl_2 solution at 298 K and (b) frozen glass at 25 K of **4** (black = experimental spectra; red = simulated spectra).

hyperfine coupling at $g = 2.003$, as depicted in panel a of Figure 7. The satellite of the experimental spectrum is assigned to an impurity. In comparison, the cis isomer **2** displays a hyperfine spectrum due to one PPh_3 ligand, as shown in panel a of Figure 8. The isotropic spectra of **3** and **4** are comparatively broad with line width 17−18 G, as depicted in the panel a of Figure 9. All of the fluid solution isotropic spectra at 2.001 ± 0.002 are consistent with the existence of organic radicals, i.e., resonating form A of the Scheme 1 as a majority. The X- and Q-band frozen glasses EPR spectra of the complexes are anisotropic. No hyperfine coupling due to PPh_3 is observed here, i.e., no spin density on two *trans*-PPh_3 ligands. The anisotropy of the EPR spectra in all of these cases is a measure of the contribution of resonating structure B in **1**−**4**. In this context, the recent report of Peters et al. on the EPR spectral features of mononuclear ruthenium(I) and osmium(I) complexes with spin density >70% at the metal center and the anisotropy of the g values ($\Delta g = g_{max} - g_{min}$) is noteworthy.[13a] The article provides guiding parameters to disclose the electronic state of a delocalized system incorporating a ruthenium(I) or osmium(I) ion. The Δg values reported in the article are about 0.15 for the two ruthenium complexes and 0.26 for the corresponding osmium complexes. These numbers are in line with large contributions of the metals to the radicals. The anisotropy of the EPR spectra of **1** (panels b and c of Figure 7), **2** (panels b and c of Figure 8), and **4** (panel b of Figure 9) is clearly templated to but comparatively less than (Δg = 0.012 for **1** and 0.028 for **4**) those reported by Peters et al. This result correlates well with a lower contribution of the metals to the radicals, as reported in the cases of lead semiquinone radical complexes.[41] Because of the larger spin−orbit coupling, the anisotropy in the osmium analogue (**4**) is higher. Thus, the EPR spectra have predicted a minor resonance contribution of the *trans*- or *cis*-$[M^{I}(PQ)(PPh_3)_2(CO)X]$ form incorporating d^7 (low-spin) metal ions in **1**−**4**. These findings are in agreement to conclude that the ground-state electronic state of these paramagnetic PQ complexes of ruthenium and osmium can be best described by a superposition of the valence tautomers, A and B, as shown in Scheme 1. However, the existence of the thermodynamic equilibrium between the forms A and B of complexes **1**−**4** has not been observed even at low temperature; i.e., no measurable electromerization/tautomerization occurred in these cases. Quantum-chemical calculations at the DFT/B3LYP level on **1** and **5**−**7** have also inferred the contribution of both resonance structures A (major) and B (minor) on the ground-state electronic state of complexes **1**−**4**.

Redox Series. The stabilities of the oxidized and reduced analogues of complexes **1**−**4** in solutions were investigated at 298 and 253 K by cyclic voltammetry experiments in CH_2Cl_2 solutions. The cyclic voltammograms are shown in Figure 10, and the redox potential data versus the ferrocenium/ferrocene, Fc^+/Fc, couple are summarized in Table 8.

Both the anodic and cathodic waves of the trans analogue **1** in CH_2Cl_2 at around 0.0 and −1.1 V are reversible, as illustrated in panel a of Figure 10, affirming the existence of both cations and anions in solution at least on the experimental time scale (defined by the scan rate) at 298 K. The electrochemistry of **3** is very similar to that of **1**, as illustrated in panel c of Figure 10, predicting its trans geometry.

In similar conditions, **2** and **4** with cis geometries display reversible oxidation and irreversible reduction waves respectively at −0.05 and −0.03 V (panels b and d of Figure 10). The trans−cis geometry and metal-independent redox potentials ($E^1_{1/2}$, Table 8) at −0.06, −0.05, +0.03, and −0.03 V of **1**−**4** have been assigned to a $PQ/PQ^{\bullet-}$ redox couple (confirmed by the isolation of an oxidized analogue, $\mathbf{1}^+I_3^-$), while the redox waves ($E^2_{1/2}$; Table 8) at −1.11 and −0.96 V respectively for **1** and **3** are assigned to $PQ^{\bullet-}/PQ^{2-}$ reduction couple. The $PQ^{\bullet-}/PQ^{2-}$ redox couple are irreversible in the cis isomers **2** and **4** even at 253 K. It is predicted that the reduction of $PQ^{\bullet-}$ to PQ^{2-} facilitates dissociation of the cis analogues. To investigate the type of dissociation, a bulk electrolysis experiment at a potential of −0.7 V was performed at 298 K and the resultant solution was analyzed by both ESI^+ and ESI^- mass spectra. The only significant peak other than $N(n\text{-}Bu)_4^+$ (ESI^+) and PF_6^- (ESI^-) mass peaks detected was assigned to the $[Ru(PQ)(PPh_3)(CO)(Cl)]^+$ ion at the ESI^+ mass spectra.

dx.doi.org/10.1021/ic300327x | *Inorg. Chem.* 2012, 51, 6687−6699

Table 7. X- and Q-Band EPR Spectral Parameters of Complexes 1−4

complex	conditions	g_{iso}/g_{av}	g_1	g_2	g_3	Δg^a	line width/G[b]
1	solid (298 K)[c]	2.001	2.005	2.005	1.993	0.012	6.7, 6.7, 8.0
	CH_2Cl_2 solution (298 K)[c]	2.002					4.3, $A(^{35,37}Cl)$ = 2.8
	CH_2Cl_2 frozen glass (25 K)[c]	2.002	2.007	2.003	1.995	0.012	9.5, 9.5, 11
	CH_2Cl_2 frozen glass (25 K)[d]	2.002	2.007	2.003	1.995	0.012	9.5, 9.5, 11
2	solid (298 K)[c]	2.002					17.3
	CH_2Cl_2 solution (298 K)[c]	2.003					6.4, $A(^{31}P)$ = 6.1
	CH_2Cl_2 frozen glass (25 K)[c]	2.003	2.008	2.004	1.997	0.011	9.5, 10.7, 14
	CH_2Cl_2 frozen glass (25 K)[d]	2.003	2.008	2.004	1.997	0.011	9.5, 10.7, 14
3	CH_2Cl_2 solution (298 K)[c]	2.000					20.1
4	CH_2Cl_2 solution (298 K)[c]	1.999					18.9
	CH_2Cl_2 frozen glass (25 K)[c]	1.998	2.008	2.008	1.980	0.028	13, 13, 26

[a] $\Delta g = g_{max} - g_{min}$. [b] Line width = peak-to-peak width of the spectrum. Line-width values were obtained from the simulation of the spectra using the *WINEPR SimFonia* program. [c] X-band EPR spectra. [d] Q-band EPR spectra.

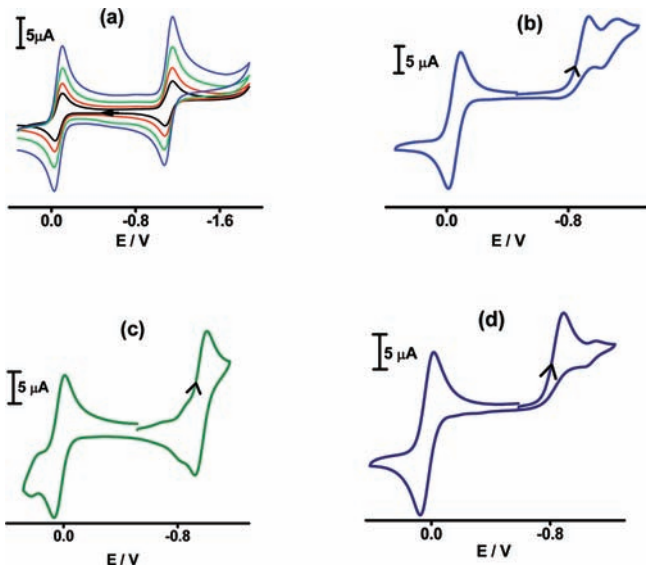

Figure 10. Cyclic voltammograms of (a) **1** [scan rate (sr): 50 (black), 100 (red), 200 (green), and 400 (blue) mV s^{-1}] at 298 K, (b) **2** (sr, 100 mV s^{-1}) at 253 K, (c) **3** (sr, 100 mV s^{-1}), and (d) **4** (sr, 100 mV s^{-1}) at 298 K in CH_2Cl_2. Conditions: 0.20 M $[N(n\text{-}Bu)_4]PF_6$ supporting electrolyte; platinum working electrode.

Table 8. Redox Potentials of Complexes 1−4 in a CH_2Cl_2 Solution (0.20 M $[N(n\text{-}Bu)_4]PF_6$) at 298 K

complex	$E_{1/2}{}^1$/V (ΔE^a/mV)	$E_{1/2}{}^2$/V (ΔE^a/mV)
1	−0.06 (80)	−1.11 (80)
2[b]	−0.05 (78)	−0.93[c]
3	+0.03 (74)	−0.96 (80)
4	−0.03 (80)	−0.88[c]

[a] Peak-to-peak separation. [b] At 253 K. [c] Cathodic peak.

This significant observation discloses that one of the paths of decomposition of $\mathbf{2}^-$ is due to PPh_3 dissociation.

No anodic waves of **1**−**4** assignable to the oxidation $M^{II/III}$ were detected in the experimental range (up to +2.0 V), and this may be due to the coordination of strong π-acidic PPh_3, CO, and PQ ligands to the metal(II) center. The electronic structures of $\mathbf{1}^+$, $\mathbf{1}^-$, $\mathbf{2}^+$, $\mathbf{3}^+$, $\mathbf{3}^-$, and $\mathbf{4}^+$, as shown in Scheme 2, have been elucidated by DFT calculations on $\mathbf{5}^+$ and $\mathbf{5}^-$ ions and are elaborated below. The electronic absorption (UV−vis/NIR) feature of the anions was investigated by spectroelectrochemical experiments.

Scheme 2. Redox Series of 1 (M = Ru, X = Cl) and 3 (M = Os, X = Br) Complexes

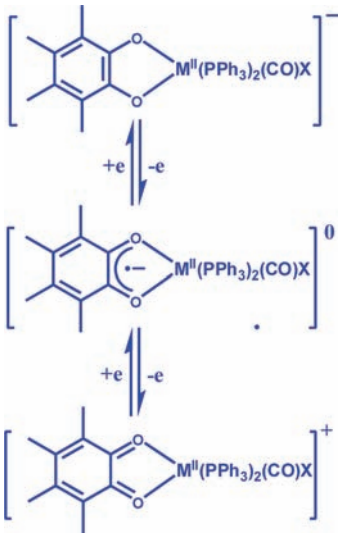

Electronic Structures of 1−4. DFT calculations on **1** and **5** with doublet spin states have elucidated the spin-density distribution and effect of the PR_3 ligand on the trans isomers **1** and **3**. The electronic structures of **2** and **4** have been established by DFT calculations on **6** and **7** at the unrestricted B3LYP level of theory. The calculated gas-phase geometrical parameters are summarized in Tables 3−5. The calculations have established the following features: (i) the spin-density distribution of the isomers is PR_3-independent; (ii) **5** is ∼17 kJ/mol lower in energy than **6**, but because the reaction has been performed in boiling toluene (383 K), both the cis and trans isomers **1** and **2** have been successfully isolated; (iii) $Ru^{II}-PMe_3$ lengths in **5** > $Ru^{II}-PMe_3$ lengths in **6**; (iv) $Ru^{II}-O$ lengths in **6** > $Ru^{II}-O$ lengths in **5**; (v) C−O lengths in **5** and **6** > C═O lengths; (vi) C−C lengths of the chelates < C(sp2)−C(sp2) lengths. Similar trends have been observed in the experimental lengths of **1**, **2**·toluene, and **4**·CH_2Cl_2 (Tables 3−5).

Mulliken spin-density analyses of **1** and **5**−**7** reveal that the spin density is predominantly localized on the PQ chelate, reducing PQ to $PQ^{\bullet-}$, as shown in Figure 11, confirming the major contribution of the resonance form A (Scheme 1) in the electronic state of **1**−**4**. The spin distribution in **1** and **5** is very similar and unperturbed by PR_3 groups. In all cases, the spin

dx.doi.org/10.1021/ic300327x | Inorg. Chem. 2012, 51, 6687−6699

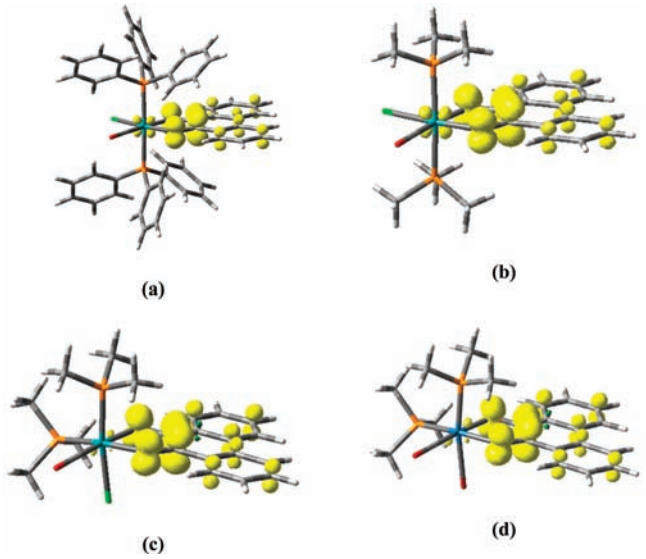

Figure 11. Spin-density plots of (a) **1**, (b) **5**, (c) **6**, and (d) **7** obtained from Mulliken spin-population analyses.

density is equally localized over carbon and oxygen atoms, revealing the electronic structure of PQ in **1**−**4**, as shown in Chart 2. These features of the spin-density distributions explain well the comparatively longer C−O and shorter C−C lengths of the OO chelate in **1**−**4**. However, the calculations have established that because of valence tautomerization the spin density to the extent of ∼6% is localized on the ruthenium and osmium ions in **1** and **5**−**7**, affirming the contribution of the resonance form B (Scheme 1) to the ground-state electronic structures of complexes **1**−**4**. This observation infers the existence of the B form, which instigates the anisotropy in the EPR spectra of complexes **1**−**4** in solid and frozen CH_2Cl_2 glasses at 25 K (Figures 7−9).

Chart 2. Electronic State of $PQ^{\bullet-}$ in Complexes 1−4[a]

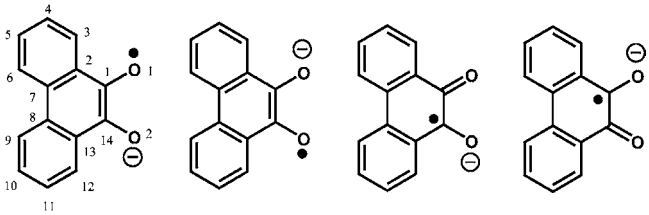

[a]Calculated Mulliken atomic spin densities in **1**: O(1), 0.19; O(2), 0.18; C(1), 0.23; C(3), 0.08; C(5), 0.08; C(7), 0.05; C(8), 0.04; C(10), 0.08; C(12), 0.07; C(14), 0.22. Calculated Mulliken atomic spin densities in **6**: O(1), 0.22; O(2), 0.21; C(1), 0.17; C(3), 0.07; C(5), 0.07; C(7), 0.03; C(8), 0.06; C(10), 0.08; C(12), 0.08; C(14), 0.20. Calculated Mulliken atomic spin densities in **7**: O(1), 0.22; O(2), 0.20; C(1), 0.16; C(3), 0.07; C(5), 0.07; C(7), 0.05; C(8), 0.06; C(10), 0.08; C(12), 0.08; C(14), 0.20.

The Ru^{II}−PPh_3 lengths in **1** and **2**·toluene are significantly different. The average Ru^{II}−PPh_3 length in **1** is comparatively longer than those in the cis isomers **2**·toluene and **4**·CH_2Cl_2. Molecular orbital analyses have shown that, in the cis isomer (**6**), multiple $d_{Ru} \rightarrow p_P$ π-back-bonding interactions with two different d orbitals of ruthenium and p orbitals of phosphorus occur, while in the trans isomer (**5**), the same d orbital interacts with two *trans*-PPh_3 groups, simultaneously resulting in a weaker and longer d → p π-back bond. This aspect of bonding features are common for cis and trans analogues in coordination complexes incorporating π-acidic ligands.

Coordination of PQ to Ruthenium(II) and Osmium(II). *trans*-$[Ru^{II}(PQ)(PPh_3)_2(CO)(Cl)]^+$ (1^+), *cis*-$[Ru^{II}(PQ)(PPh_3)_2(CO)(Cl)]^+$ (2^+), *trans*-$[Os^{II}(PQ)(PPh_3)_2$ $(CO)(Br)]^+$ (3^+), *cis*-$[Os^{II}(PQ)(PPh_3)_2$ $(CO)(Br)]^+$ (4^+). The electronic structure of cations was analyzed by the restricted DFT calculations on 5^+ using a singlet spin state. The bond parameters of the optimized geometry of 5^+ are listed in Table 6. Two shorter C−O lengths and a longer C−C length of the OO chelate correlate well with those obtained from the single-crystal X-ray structure determination of $1^+I_3^-$ (Table 6) and are consistent with the neutral PQ description.[21] These trends of bond parameters are quite different from those obtained from the single-crystal X-ray structures of **1**, **2**·toluene, and **4**·CH_2Cl_2 and DFT calculations on **5** and **6** incorporating a 9,10-phenanthrenesemiquinone radical ($PQ^{\bullet-}$) chelate. It signifies that the reversible redox waves of **1**−**4** respectively at −0.06, −0.05, +0.03, and −0.03 V are due to a $PQ/PQ^{\bullet-}$ redox couple, and the one-electron-oxidized analogues have been described as the neutral PQ complexes of ruthenium(II)/osmium(II) as 1^+, 2^+, 3^+, and 4^+. Stability analysis has proved that the singlet solution of 5^+ is stable without any triplet perturbation and does not display any closed-shell singlet−open-shell singlet perturbation. Thus, complexes 1^+, 2^+, 3^+, and 4^+ are examples of neutral PQ chelation to ruthenium(II) and osmium(II) metal ions, as observed in $[Cu(dppf)(PQ)]BF_4$.[21]

Coordination of 9,10-Phenanthrenediolato (PQ^{2-}) to Ruthenium(II) and Osmium(II). *trans*-$[Ru^{II}(PQ^{2-})(PPh_3)_2(CO)(Cl)]^-$ (1^-) and *trans*-$[Os^{II}(PQ^{2-})(PPh_3)_2(CO)(Br)]^-$ (3^-). The geometry of 5^- at the RB3LYP level of theory was optimized with the singlet spin state to account for the electronic structures of 1^- and 3^-. The calculated bond parameters are summarized in Table 9. The C−O and C−C length trend of the OO chelate is different here and is reverse to those found in 1^+. Comparatively, longer C−O and shorter C−C bond lengths of the OO chelate conclude the presence of the reduced dianionic PQ^{2-} ligand in 1^-. Thus, the redox waves of **1** and **3** at −1.11 and −0.96 V referenced versus Fc^+/Fc have been defined as the reduction of the monoanionic anion radical $PQ^{\bullet-}$ to the dianionic PQ^{2-} ligand. In cases of cis isomers, this reduction process is irreversible.

Table 9. Calculated Bond Lengths (Å) of the PQ and PQ^{2-} Chelates in 5^+ and 5^- Ions

	5^+	5^-	
	PQ	PQ^{2-}	
C(1)-O(1)	1.256	1.333	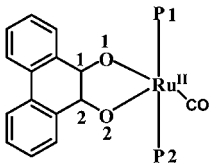
C(1)-O(2)	1.261	1.333	
C(1)-C(2)	1.492	1.400	
Ru-O(1)	2.211	2.153	
Ru-O(2)	2.094	2.107	
Ru-P(1)	2.449	2.390	
Ru-P(2)	2.449	2.392	

Elucidation of Electronic Structures of the Reported Complexes. This work with the support of the reported results[19−22] proved that calculated bond parameters of the OO

dx.doi.org/10.1021/ic300327x | *Inorg. Chem.* 2012, 51, 6687−6699

chelate of the PQ ligand are convincing tools to analyze the electronic states of its complexes. The established trend of the bond parameters of PQ, $PQ^{\bullet-}$, and PQ^{2-} is useful to reevaluate the electronic structures of the PQ complexes reported some time back. In this regard, the molecular and electronic structures of $M^0(CO)_3$(chrysenequinone) complexes[23] achieved upon a substitution reaction of $M(CO)_5$ or $Ru^{IV}(PQ)(PPh_3)_2X_2$ families[24] afforded upon oxidative addition of PQ to $Ru(PPh_3)_3X_2$ (M = Ru, Os; X = Cl, Br) are subjects of discussions. The reported geometry of $M^0(CO)_3$(chrysenequinone) is a trigonal bipyramid (tbp) with the neutral PQ ligand at the equatorial position. Geometry optimization of the $Ru(CO)_3$(chrysenequinone) complex at the B3LYP/DFT level of theory, as used for calculations of complexes **1**−**4**, has established that the square-pyramidal geometry is more stable (by 80 kJ/mol) compared to that of the reported trigonal-bipyramidal geometry (Table S7, Supporting Information). It authenticates the square-pyramidal geometry of $M(CO)_3$(chrysenequinone) families, as shown in Chart 3. It is noted that the HOMO is composed of both

Chart 3. Optimized Geometry and Electronic State of $Ru(CO)_3$(chrysenequinone)[a]

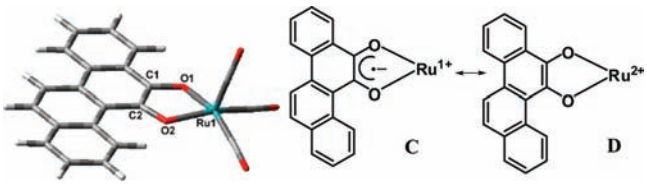

[a]Select calculated bond lengths (Å) are as follows: Ru1−CO_{ax}, 1.922; Ru1−CO_{eq}, 1.937; Ru1−O1, 2.033; Ru1−O2, 2.033; C1−O1, 1.312; C2−O2, 1.312; C1−C2, 1.415.

ruthenium and ligand orbitals with the singlet-to-triplet perturbation Hessian eigenvalue, 0.0004. The calculated bond parameters do not support the quinone state of the bidentate ligand. The significant calculated bond parameters of the OO chelate of the $Ru(CO)_3$(chrysenequinone) complex are listed in Chart 3. This length trend and the features of HOMO does not correlate with the presence of a neutral chrysenequinone but is more consistent with an electronic state obtained after superposition of the resonance structures C, chrysenesemiquinone complexes of ruthenium(I) and D, and the chrysenediolato complex of ruthenium(II), as depicted in Chart 3. Similarly, the oxidative addition of PQ to ruthenium(II) phosphine complexes, affording ruthenium(IV) and 9,10-phenanthrenediolato, is questionable. Studies of the molecular and electronic structures of the series of PQ complexes of the type $M(PQ)(PPh_3)_2X_2$ (M = Ru, Os, Rh) have concluded the presence of the monoanionic $PQ^{\bullet-}$ ligand coordinated to a metal(III) ion in $M(PQ)(PPh_3)_2X_2$ families.[42]

Electronic Absorption Spectra. The origins of geometry-dependent electronic spectra of **1**−**4** were elucidated by TD DFT calculations on **5**−**7** with doublet spin states. The UV−vis/NIR spectral features of the oxidized ($\mathbf{1}^+I_3^-$) and reduced ($\mathbf{1}^-$) analogues were also investigated by TD DFT calculations on singlet $\mathbf{5}^+$ and $\mathbf{5}^-$ ions. The calculated results are listed in Table 10. The calculations summarized that the low-energy absorption bands above 500 nm in **1**−**4** or $\mathbf{1}^+$ are due to metal-to-ligand charge transfer or mixed-metal halide (X)-to-ligand charge transfer.

The most significant unoccupied photoactive π_{PQ}* orbital of the trans isomer is more stabilized compared to that of the cis isomer. The electronic spectra of the trans analogues (**1** and **3**) are similar but are different from those of the cis analogues (**2** and **4**). The low-energy absorption band above 600 nm is absent in the cis analogue. TD DFT calculations have assigned the mixed-metal chloride-to-ligand charge transfer (MMClLCT) as the origin of this low-energy band above 600 nm (Table 10) for the trans complexes. The charge-transfer process involves the ruthenium d_{yz} orbital (β-HOMO) in the trans isomer, while the MMClLCT process in the cis geometry involves the ruthenium d_{xz} (β-HOMO−1) and less stabilized π_{PQ}* (LUMO) orbitals shifting the absorption maxima to the higher energy (<600 nm) as shown in Figure 1. The DFT calculations have established that both the photoactive ruthenium d_{yz} (HOMO) and π_{PQ}* (LUMO) orbitals of **1** are stabilized in $\mathbf{1}^+$, shifting the MMClLCT process to lower energy. The calculated lower-energy band at 685 nm of **5** is red-shifted to 819 nm in $\mathbf{5}^+$. The same absorption features have been observed in $\mathbf{1}^+I_3^-$ (Table 2 and Figure 2). The one-electron-reduced analogue, $\mathbf{1}^-$, was not successfully isolated. However, the change of the absorption features upon one-electron reduction of **1** to $\mathbf{1}^-$ was recorded by spectroelectrochemistry measurement (Figure 12). The reverse trend is observed in this reductive transformation, blueshifting the λ_{max} to 618 nm (Figure 12). In the reduced anion, the doubly occupied π_{PQ}* orbital is HOMO and the transition from this HOMO to another ligand-based unoccupied orbital is the origin of absorption. Upon reduction of **1** to $\mathbf{1}^-$, the MMClLCT band above 600 nm disappears. The origins of higher-energy absorption band maxima of all of the complexes are listed in Table 10. The higher-energy band maxima at 400−430 nm have the origin of mixed-metal−ligand-to-ligand charge transfer (MMLLCT). In both the cases of oxidation and reduction, the MMLLCT band at 400 nm remains unaltered.

■ CONCLUSIONS

Coordination of redox-noninnocent PQ to the redox-active ruthenium(II) and osmium(II) metal ions generating paramagnetic isomeric species of the type *trans*- and *cis*-$[M(PQ)(PPh_3)_2(CO)X]$ has been substantiated by single-crystal X-ray structure determinations, EPR spectra, and DFT calculations (M = Ru, X = Cl; M = Os, X = Br). The electronic state of $[M(PQ)(PPh_3)_2(CO)X]$ complexes has been defined by the two resonating forms, $[M^{II}(PQ^{\bullet-})(PPh_3)_2(CO)X]$ and $[M^{I}(PQ)(PPh_3)_2(CO)X]$, respectively as major and minor components. No measurable thermodynamic equilibria between two resonating structures have been detected. *trans*-$[M(PQ)(PPh_3)_2(CO)X]$ complexes undergo one-electron oxidation relatively at low potentials, affording $\mathbf{1}^+$ and $\mathbf{3}^+$ neutral PQ complexes of metal(II), and one-electron reduction, furnishing $\mathbf{1}^-$ and $\mathbf{3}^-$ dianionic 9,10-phenanthrenediolato complexes of metal(II). The X-ray bond parameters of the isolated oxidized congener $\mathbf{1}^+I_3^-$ are consistent with PQ coordination to the ruthenium(II) ion. Although the reduction processes of the *cis*-$[M(PQ)(PPh_3)_2(CO)X]$ analogues are irreversible, the oxidation processes are reversible, generating neutral PQ complexes of ruthenium(II)/osmium(II), such as $\mathbf{2}^+$ and $\mathbf{4}^+$. Significant observations of the study are as follows: (i) all of the anionic complexes are PQ^{2-} complexes of ruthenium(II)/osmium(II); (ii) all of the cationic complexes are neutral PQ complexes of ruthenium(II)/osmium(II); (iii) the ground-state electronic structure of the neutral complexes is

dx.doi.org/10.1021/ic300327x | Inorg. Chem. 2012, 51, 6687−6699

Table 10. Excitation Energies (λ/nm), Oscillator Strengths (f), Transition Types, and Dominant Contributions of UV−Vis/NIR Absorption Bands of 5, 6, 5^+, and 5^- Obtained from TD DFT Calculations

λ_{calc}/nm	f	λ_{exp}/nm	significant contributions (>10%)	transition types	dominant contributions
			5 (Corresponds to Experimental Data of **1**)		
685	0.048	734	β-HOMO → LUMO (96%)	d_{Ru} (53%) + p_{Cl} (29%) → π_L^* (92%)	MMClLCT
534	0.018	592	β-HOMO−2 → LUMO (94%)	π_L (94) → π_L^* (92)	$\pi_{PQ} \rightarrow \pi_{PQ}^*$
474	0.063	475	β-HOMO−3 → LUMO (86%)	p_{Ru} (14) + p_{Cl+P} (60) → π_L^* (92)	MMLLCT
447	0.015		α-HOMO → LUMO (96%)	π_L (88) → π_L^* (100)	$\pi_{PQ} \rightarrow \pi_{PQ}^*$
443	0.029		α-HOMO → LUMO+1 (67%)	π_L (88) → π_L^* (99)	$\pi_{PQ} \rightarrow \pi_{PQ}^*$
434	0.023	412	β-HOMO−4 → LUMO (76%)	d_{Ru} (32) + p_P (10) + π_L(43) → π_L^* (92)	MMLLCT
392	0.026		β-HOMO−5 → LUMO (81%)	d_{Ru} (23) + π_L (64) → π_L^* (92)	MMLLCT
			6 (Corresponds to Experimental Data of **2**)		
534	0.018	612	β-HOMO−2 → LUMO (29%)	π_L (91) →π_L^* (95)	$\pi_{PQ} \rightarrow \pi_{PQ}^*$
		567	β-HOMO−1 → LUMO (57%)	d_{Ru} (25) + p_{Cl} (64) → π_L^* (95)	MMClLCT
		508			
438	0.020	475	α-HOMO → LUMO (21%)	π_L (93) → π_L^* (99)	$\pi_{PQ} \rightarrow \pi_{PQ}^*$
			α-HOMO → LUMO+2 (36%)	π_L (93) → π_L^* (22) + d_{Ru} (31) + p_P(37)	LMMLCT
427	0.087		α-HOMO → LUMO (11%)	π_L (93) → π_L^* (99)	$\pi_{PQ} \rightarrow \pi_{PQ}^*$
			β-HOMO−4 → LUMO (66%)	d_{Ru} (11) + p_{Cl} (27) + π_L (57) → π_L^* (95)	MMLLCT
414	0.049	408	β-HOMO−5 → LUMO (66%)	π_L (74) + p_{Cl} (14) → π_L^* (95)	MClLLCT
			5^+ (Corresponds to Experimental Data of $1^+I_3^-$)		
819	0.045	820	HOMO → LUMO (74%)	d_{Ru} (44) + p_{Cl} (44) → π_L^* (86)	MMClLCT
619	0.050	610	HOMO−3 → LUMO (46%)	π_L (98) → π_L^* (86)	$\pi_{PQ} \rightarrow \pi_{PQ}^*$
			HOMO−2 → LUMO (43%)	d_{Ru} (17) + p_{Cl+P} (68) + π_L (14) → π_L^* (86)	MMLLCT
596	0.134		HOMO−3 → LUMO (46%)	π_L (98) → π_L^* (86)	$\pi_{PQ} \rightarrow \pi_{PQ}^*$
			HOMO−2 → LUMO (36%)	d_{Ru} (17) + p_{Cl+P} (68) + π_L (14) → π_L^* (86)	MMLLCT
517	0.075	505	HOMO−4 → LUMO (82%)	d_{Ru} (53) + π_{CO} (10) + π_L (28) → π_L^* (86)	MMLLCT
415	0.042		HOMO−5 → LUMO (83%)	d_{Ru} (14) + π_L (77) → π_L^* (86)	MMLLCT
			5^- (Corresponds to Experimental Data of 1^-)		
557	0.017	618	HOMO → LUMO (94%)	π_L(92)→π_L^*(99)	LLCT
438	0.102	410	HOMO → LUMO+3 (78%)	π_L (92) → π_L^* (98)	LLCT

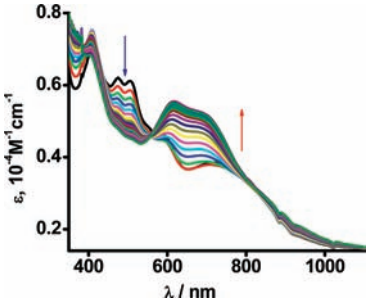

Figure 12. Spectroelectrochemistry of **1** showing the electronic spectrum of electrochemically generated 1^- in CH_2Cl_2 at 298 K.

best described by a superposition of the valence tautomeric states of $PQ^{\bullet-}$ coordinated to ruthenium(II)/osmium(II) and PQ coordinated to ruthenium(I)/osmium(I) ions; (iv) the $PQ^{\bullet-}/PQ^{2-}$ redox couple is irreversible even at 253 K in the cis isomer, inferring the nonexistence of PQ^{2-} complexes of cis analogues due to PPh_3 dissociation.

■ ASSOCIATED CONTENT

Supporting Information

X-ray crystallographic CIF files for complexes **1**, **2**·toluene, **4**·CH_2Cl_2, and $1^+I_3^-$, IR spectra of **1** and $1^+I_3^-$ (Figure S1), optimized geometry of Ru(chrysenequinone)$(CO)_3$ (Figure S2), and optimized coordinates of **1**, **5**, **6**, **7**, 5^+, 5^-, and Ru(chrysenequinone)$(CO)_3$ (Tables S1−S7). This material is available free of charge via the Internet at http://pubs.acs.org.

■ AUTHOR INFORMATION

Corresponding Author

*E-mail: ghosh@pghosh.in. Phone: +91-33-2428-7347. Fax: +91-33-2477-3597.

Notes

The authors declare no competing financial interest.

■ ACKNOWLEDGMENTS

Financial support received from the DST (Grant SR/S1/IC-10/2008) and UGC (Grant 34-315/2008 (SR)), New Delhi, India, is acknowledged.

■ REFERENCES

(1) (a) Pierpont, C. G.; Buchanan, R. M. *Coord. Chem. Rev.* **1981**, *38*, 45. (b) Frey, P. A. *Chem. Rev.* **1990**, *90*, 1343. (c) Stubbe, J.; Van der Donk, W. A. *Chem. Rev.* **1998**, *98*, 705. (d) Khusniyarov, M. M.; Weyhermüller, T.; Bill, E.; Wieghardt, K. *J. Am. Chem. Soc.* **2009**, *131*, 1208. (e) Lu, C. C.; Bill, E.; Weyhermüller, T.; Bothe, E.; Wieghardt, K. *J. Am. Chem. Soc.* **2008**, *130*, 3181.

(2) (a) Pierpont, C. G.; Lange, C. W. *Prog. Inorg. Chem.* **1994**, *41*, 331. (b) Barthram, A. M.; Cleary, R. L.; Kowallick, R.; Ward, M. D. *Chem. Commun.* **1998**, 2695. (c) García-Cañadas, J.; Meacham, A. P.; Peter, L. M.; Ward, M. D. *Angew. Chem., Int. Ed.* **2003**, *42*, 3011. (d) Okamura, R.; Wada, T.; Aikawa, K.; Nagata, T.; Tanaka, K. *Inorg. Chem.* **2004**, *43*, 7210. (e) Wada, T.; Muckerman, J. T.; Fujita, E.; Tanaka, K. *Dalton Trans.* **2011**, *40*, 2225.

(3) (a) Chun, H.; Verani, C. N.; Chaudhuri, P.; Bothe, E.; Bill, E.; Weyhermuller, T.; Wieghardt, K. *Inorg. Chem.* **2001**, *40*, 4157. (b) Chun, H.; Weyhermüller, T.; Bill, E.; Wieghardt, K. *Angew. Chem., Int. Ed.* **2001**, *40*, 2489. (c) Bhattacharya, S.; Gupta, P.; Basuli, F.; Pierpont, C. G. *Inorg. Chem.* **2002**, *41*, 5810. (d) Das, D.; Das, A. K.;

Sarkar, B.; Mondal, T. K.; Mobin, S. M.; Fiedler, J.; Zalis, S.; Urbanos, F. A.; Jimenez-Aparicio, R.; Kaim, W.; Lahiri, G. K. *Inorg. Chem.* **2009**, *48*, 11853. (e) Roy, A. S.; Saha, P.; Adhikary, N. D.; Ghosh, P. *Inorg. Chem.* **2011**, *50*, 2488.

(4) (a) Balch, A. L.; Holm, R. H. *J. Am. Chem. Soc.* **1966**, *88*, 5201. (b) Carugo, O.; Djinovic, K.; Rizzi, M.; Castellani, B. C. *J. Chem. Soc., Dalton Trans.* **1991**, 1551. (c) Herebian, D.; Bothe, E.; Neese, F.; Weyhemuller, T.; Wieghardt, K. *J. Am. Chem. Soc.* **2003**, *125*, 9116. (d) Ghosh, P.; Begum, A.; Herebian, D.; Bothe, E.; Hildenbrand, P.; Weyhermuller, T.; Wieghardt, K. *Angew. Chem., Int. Ed.* **2003**, *42*, 563. (e) Chlopek, K.; Bill, E.; Weyhermuller, T.; Wieghardt, K. *Inorg. Chem.* **2005**, *44*, 7087.

(5) (a) Ghosh, P.; Bill, E.; Weyhermuller, T.; Wieghardt, K. *J. Am. Chem. Soc.* **2003**, *125*, 3967. (b) Herebian, D.; Bothe, E.; Bill, E.; Weyhermüller, T.; Wieghardt, K. *J. Am. Chem. Soc.* **2001**, *123*, 10012. (c) Roy, N.; Sproules, S.; Bill, E.; Weyhermüller, T.; Wieghardt, K. *Inorg. Chem.* **2008**, *47*, 10911.

(6) (a) Sokolowski, A.; Müller, J.; Weyhermüller, T.; Schnepf, R.; Hildebrandt, P.; Hildenbrand, K.; Bothe, E.; Wieghardt, K. *J. Am. Chem. Soc.* **1997**, *119*, 8889. (b) Wang, Y.; DuBois, J. L.; Hedman, B.; Hodgson, K. O.; Stack, T. D. P. *Science* **1998**, *279*, 537. (c) Chaudhuri, P.; Wieghardt, K. *Prog. Inorg. Chem.* **2001**, *50*, 151.

(7) Penkert, F. N.; Weyhemuller, T.; Bill, E.; Hildebrandt, P.; Lecomte, S.; Wieghardt, K. *J. Am. Chem. Soc.* **2000**, *122*, 9663.

(8) Buttner, T.; Geier, J.; Frison, G.; Harmer, J.; Calle, C.; Schweiger, A.; Schonberg, H.; Grutzmacher, H. *Science* **2005**, *307*, 235.

(9) Kimura, S.; Bill, E.; Bothe, E.; Weyhemuller, T.; Wieghardt, K. *J. Am. Chem. Soc.* **2001**, *123*, 6025.

(10) (a) Shivakumar, M.; Pramanik, K.; Ghosh, P.; Chakravorty, A. *Inorg. Chem.* **1998**, *37*, 5968. (b) Pramanik, K.; Shivakumar, M.; Ghosh, P.; Chakravorty, A. *Inorg. Chem.* **2000**, *39*, 195. (c) Schwach, M.; Hausen, H. D.; Kaim, W. *Inorg. Chem.* **1999**, *38*, 2242. (d) Joy, S.; Krämer, T.; Paul, N. D.; Banerjee, P.; McGrady, J. E.; Goswami, S. *Inorg. Chem.* **2011**, *50*, 9993. (e) Samanta, S.; Ghosh, P.; Goswami, S. *Dalton Trans.* **2012**, *41*, 2213.

(11) (a) Gardiner, M. G.; Hanson, G. R.; Henderson, M. J.; Lee, F. C.; Raston, L. C. *Inorg. Chem.* **1994**, *33*, 2456. (b) Muresan, N.; Lu, C. C.; Ghosh, M.; Peters, J. C.; Abe, M.; Henling, L. M.; Bill, E.; Wieghardt, K. *Inorg. Chem.* **2008**, *47*, 4579.

(12) Patra, S. C.; Biswas, M. K.; Maity, A. N.; Ghosh, P. *Inorg. Chem.* **2011**, *50*, 1331.

(13) (a) Takaoka, A.; Gerber, L. C. H.; Peters, J. C. *Angew. Chem., Int. Ed.* **2010**, *49*, 4088. (b) Puschmann, F. F.; Harmer, J.; Stein, D.; Rüegger, H.; Bruin, B. D.; Grützmacher, H. *Angew. Chem., Int. Ed.* **2010**, *49*, 385 and relevant references therein..

(14) (a) Op't Holt, B. T.; Vance, M. A.; Mirica, L. M.; Heppner, D. E.; Stack, T. D. P.; Solomon, E. I. *J. Am. Chem. Soc.* **2009**, *131*, 6421. (b) Pierpont, C. G.; Lange, C. W. The Chemistry of Transition Metal Complexes Containing Catechol and Semiquinone Ligands. In *Progress in Inorganic Chemistry*; Karlin, K. D., Ed.; John Wiley & Sons, Inc.: Hoboken, NJ, 2007; Vol. *41*, pp 331−442. (c) Kapre, R. R.; Bothe, E.; Weyhermüller, T.; DeBeer George, S.; Muresan, N.; Wieghardt, K. *Inorg. Chem.* **2007**, *46*, 7827. (d) Chouchane, S.; Wooten, J. B.; Tewes, F. J.; Wittig, A.; Müller, B. P.; Veltel, D.; Diekmann, J. *Chem. Res. Toxicol.* **2006**, *19*, 1602. (e) Wada, T.; Yamanaka, M.; Fujihara, T.; Miyazato, Y.; Tanaka, K. *Inorg. Chem.* **2006**, *45*, 8887. (f) Gorelsky, S. I.; Dodsworth, E. S.; Lever, A. B. P.; Vlcek, A. A. *Coord. Chem. Rev.* **1998**, *174*, 469.

(15) (a) Kundu, T.; Sarkar, B.; Mondal, T. K.; Mobin, S. M.; Urbanos, F. A.; Fiedler, J.; Jimnez-Aparicio, R.; Kaim, W.; Lahiri, G. K. *Inorg. Chem.* **2011**, *50*, 4753. (b) Piskunov, A. V.; Maleeva, A. V.; Fukin, G. K.; Baranov, E. V.; Bogomyakov, A. S.; Cherkasov, V. K.; Abakumov, G. A. *Dalton Trans.* **2011**, *40*, 718. (c) Bhattacharya, D.; Sathiyendiran, M.; Wu, J.-Y.; Chang, C.-H.; Huang, S.-C.; Zeng, Y.-L.; Lin, C.-Y.; Thanasekaran, P.; Lin, B.-C.; Hsu, C.-P.; Lee, G.-H.; Peng, S.-M.; Lu, K.-L. *Inorg. Chem.* **2010**, *49*, 10264. (d) Yuasa, J.; Suenobu, T.; Fukuzumi, S. *ChemPhysChem* **2006**, *7*, 942. (e) Pierpont, C. G. *Coord. Chem. Rev.* **2001**, *219−221*, 415. (f) Pierpont, C. G.; Attia, A. S. *Collect. Czech. Chem. Commun.* **2001**, *66*, 33. (g) da Cunha, C. J.; Dodsworth, E. S.; Monteiro, M. A.; Lever, A. B. P. *Inorg. Chem.* **1999**, *38*, 5399. (h) Brown, M. A.; McGarvey, B. R.; Ozarowski, A.; Tuck, D. G. *Inorg. Chem.* **1996**, *35*, 1560.

(16) (a) Sugimoto, R.; Kumagai, Y.; Nakai, Y.; Ishii, T. *Free Radical Biol. Med.* **2005**, *38*, 388. (b) Sagai, M.; Saito, H.; Ichinose, T.; Kodama, M.; Mori, Y. *Free Radical Biol. Med.* **1993**, *14*, 37. (c) Kumagai, Y.; Koide, S.; Taguchi, K.; Endo, A.; Nakai, Y.; Yoshikawa, T.; Shimojo, N. *Chem. Res. Toxicol.* **2002**, *15*, 483.

(17) Milko, P.; Roithová, J. *Inorg. Chem.* **2009**, *48*, 11734.

(18) (a) Pierpont, C. G.; Kitagawa, S. Valence Tautomerism of Metal Complexes. In *Inorganic Chromotropism: Basic Concepts and Applications of Colored Materials*; Fukuda, Y., Ed.; Elsevier: Tokyo, 2007; pp 116−142. (b) Hendrickson, D. N.; Pierpont, C. G. Valence Tautomeric Transition Metal Complexes. In *Topics in Current Chemistry*; Gütlich, P., Goodwin, H. A., Eds.; Springer-Verlag: Berlin, 2004; Vol. *234*, pp 63−95. (c) Pierpont, C. G. *Coord. Chem. Rev.* **2001**, *216−217*, 99. (d) Speier, G.; Tyeklár, Z.; Tóth, P.; Speier, E.; Tisza, S.; Rockenbauer, A.; Whalen, A. M.; Alkire, N.; Pierpont, C. G. *Inorg. Chem.* **2001**, *40*, 5653.

(19) (a) Speier, G.; Tisza, S.; Rockenbauer, A.; Boone, S. R.; Pierpont, C. G. *Inorg. Chem.* **1992**, *31*, 1017. (b) Pierpont, C. G.; Downs, H. H. *Inorg. Chem.* **1977**, *16*, 2970. (c) Pierpont, C. G.; Buchanan, R. M. *J. Am. Chem. Soc.* **1975**, *97*, 6450. (d) Pierpont, C. G.; Buchanan, R. M. *J. Am. Chem. Soc.* **1975**, *97*, 4912. (e) Batsanov, A. S.; Howard, J. A. K.; Brown, M. A.; McGarvey, B. R.; Tuck, D. G. *Chem. Commun.* **1997**, 699.

(20) (a) Hutchinson, D. A.; Chen, K. S.; Russell, J.; Wan, J. K. S. *J. Chem. Phys.* **1980**, *73*, 1862. (b) Leirer, M.; Knör, G.; Vogler, A. *Z. Naturforsch.* **1999**, *54b*, 1039. (c) Crowley, P. J.; Haendler, H. M. *Inorg. Chem.* **1962**, *1*, 904. (d) Leirer, M.; Knör, G.; Vogler, A. *Z. Naturforsch.* **1999**, *54b*, 1039. (e) Broadley, K.; Connelly, N. G.; Geiger, W. E. *J. Chem. Soc., Dalton Trans.* **1983**, 121. (f) Wang, S. R.; Cheng, C. P.; Ho, T.-I. *J. Chem. Soc., Dalton Trans.* **1988**, 2695. (g) Ho, T.-I.; Chang, C.-M.; Wang, S. R.; Cheng, C. P. *J. Chem. Soc., Dalton Trans.* **1988**, 123. (h) Brechin, E. K.; Calucci, L.; Englert, U.; Margheriti, L.; Pampaloni, G.; Pinzino, C.; Prescimone, A. *Inorg. Chim. Acta* **2008**, *361*, 2375. (i) Weir, D.; Wan, J. K. S. *J. Organomet. Chem.* **1981**, *220*, 323. (j) Foster, T.; Chen, K. S.; Wan, J. K. S. *J. Organomet. Chem.* **1980**, *184*, 113.

(21) Roy, S.; Sarkar, B.; Bubrin, D.; Niemeyer, M.; Zli, S.; Lahiri, G. K.; Kaim, W. *J. Am. Chem. Soc.* **2008**, *130*, 15230.

(22) (a) Kaim, W. *Coord. Chem. Rev.* **1987**, *76*, 187. (b) Floriani, C.; Henzi, R.; Calderazzo, F. *J. Chem. Soc., Dalton Trans.* **1972**, 2640.

(23) Ramadan, R. M. *J. Coord. Chem.* **1997**, *42*, 181.

(24) (a) Balch, A. L.; Sohn, Y. S. *J. Organomet. Chem.* **1971**, *30*, C31. (b) Girgis, A. Y.; Sohn, Y. S.; Balch, A. L. *Inorg. Chem.* **1975**, *14*, 2327. (c) Gandolfi, O.; Giovannitti, B.; Ghedini, M.; Dolcetti, G. *J. Organomet. Chem.* **1976**, *104*, C41. (d) Giovannitti, B.; Gandolfi, O.; Ghedini, M.; Dolcetti, G. *J. Organomet. Chem.* **1977**, *129*, 207.

(25) Ahmad, N.; Levison, J. J.; Robinson, S. D.; Uttley, M. F. *Inorg. Synth.* **1974**, *15*, 45.

(26) Sheldrick, G. M. *SHELXS97*; Universität Göttingen: Göttingen, Germany, 1997. (b) Sheldrick, G. M. *SHELXL97*; Universität Göttingen: Göttingen, Germany, 1997.

(27) Frisch, M. J.; Trucks, G. W.; Schlegel, H. B.; Scuseria, G. E.; Robb, M. A.; Cheeseman, J. R.; Montgomery, J. A., Jr.; Vreven, T.; Kudin, K. N.; Burant, J. C.; Millam, J. M.; Iyengar, S. S.; Tomasi, J.; Barone, V.; Mennucci, B.; Cossi, M.; Scalmani, G.; Rega, N.; Petersson, G. A.; Nakatsuji, H.; Hada, M.; Ehara, M.; Toyota, K.; Fukuda, R.; Hasegawa, J.; Ishida, M.; Nakajima, T.; Honda, Y.; Kitao, O.; Nakai, H.; Klene, M.; Li, X.; Knox, J. E.; Hratchian, H. P.; Cross, J. B.; Bakken, V.; Adamo, C.; Jaramillo, J.; Gomperts, R.; Stratmann, R. E.; Yazyev, O.; Austin, A. J.; Cammi, R.; Pomelli, C.; Ochterski, J. W.; Ayala, P. Y.; Morokuma, K.; Voth, G. A.; Salvador, P.; Dannenberg, J. J.; Zakrzewski, V. G.; Dapprich, S.; Daniels, A. D.; Strain, M. C.; Farkas, O.; Malick, D. K.; Rabuck, A. D.; Raghavachari, K.; Foresman, J. B.; Ortiz, J. V.; Cui, Q.; Baboul, A. G.; Clifford, S.; Cioslowski, J.; Stefanov, B. B.; Liu, G.; Liashenko, A.; Piskorz, P.; Komaromi, I.; Martin, R. L.; Fox, D. J.; Keith, T.; Al-Laham, M. A.; Peng, C. Y.;

Nanayakkara, A.; Challacombe, M.; Gill, P. M. W.; Johnson, B.; Chen, W.; Wong, M. W.; Gonzalez, C.; Pople, J. A. *Gaussian 03*, revision E.01; Gaussian, Inc.: Wallingford, CT, 2004.
(28) (a) *The Challenge of d and f Electrons*; Salahub, D. R., Zerner, M. C., Eds.; American Chemical Society: Washington, DC, 1989. (b) Parr, R. G.; Yang, W. *Density Functional Theory of Atoms and Molecules*; Oxford University Press: Oxford, U.K., 1989. (c) Kohn, W.; Sham, L. J. *Phys. Rev.* **1965**, *140*, A1133. (d) Hohenberg, P.; Kohn, W. *Phys. Rev.* **1964**, *136*, B864.
(29) (a) Stratmann, R. E.; Scuseria, G. E.; Frisch, M. *J. Chem. Phys.* **1998**, *109*, 8218. (b) Casida, M. E.; Jamoroski, C.; Casida, K. C.; Salahub, D. R. *J. Chem. Phys.* **1998**, *108*, 4439. (c) Bauernschmitt, R.; Ahlrichs, R. *Chem. Phys. Lett.* **1996**, *256*, 454.
(30) (a) Becke, A. D. *J. Chem. Phys.* **1993**, *98*, 5648. (b) Miehlich, B.; Savin, A.; Stoll, H.; Preuss, H. *Chem. Phys. Lett.* **1989**, *157*, 200. (c) Lee, C.; Yang, W.; Parr, R. G. *Phys. Rev. B* **1988**, *37*, 785.
(31) Pulay, P. *J. Comput. Chem.* **1982**, *3*, 556.
(32) Schlegel, H. B.; McDouall, J. J. *Computational Advances in Organic Chemistry*; Ogretir, C., Csizmadia, I. G., Eds.; Kluwer Academic: Amsterdam, The Netherlands, 1991; p 167.
(33) Hay, P. J.; Wadt, W. R. *J. Chem. Phys.* **1985**, *82*, 270.
(34) Wadt, W. R.; Hay, P. J. *J. Chem. Phys.* **1985**, *82*, 284.
(35) Hay, P. J.; Wadt, W. R. *J. Chem. Phys.* **1985**, *82*, 299.
(36) (a) Rassolov, V. A.; Ratner, M. A.; Pople, J. A.; Redfern, P. C.; Curtiss, L. A. *J. Comput. Chem.* **2001**, *22*, 976. (b) Francl, M. M.; Pietro, W. J.; Hehre, W. J.; Binkley, J. S.; DeFrees, D. J.; Pople, J. A.; Gordon, M. S. *J. Chem. Phys.* **1982**, *77*, 3654. (c) Hariharan, P. C.; Pople, J. A. *Mol. Phys.* **1974**, *27*, 209. (d) Hariharan, P. C.; Pople, J. A. *Theor. Chim. Acta* **1973**, *28*, 213. (e) Hehre, W. J.; Ditchfield, R.; Pople, J. A. *J. Chem. Phys.* **1972**, *56*, 2257.
(37) (a) Clark, T.; Chandrasekhar, J.; Spitznagel, G. W.; Schleyer, P. v. R. *J. Comput. Chem.* **1983**, *4*, 294. (b) Hariharan, P. C.; Pople, J. A. *Theor. Chim. Acta* **1973**, *28*, 213.
(38) O'Boyle, N. M.; Tenderholt, A. L.; Langner, K. M. *J. Comput. Chem.* **2008**, *29*, 839.
(39) (a) Cossi, M.; Rega, N.; Scalmani, G.; Barone, V. *J. Comput. Chem.* **2003**, *24*, 669. (b) Barone, V.; Cossi, M. *J. Phys. Chem. A* **1998**, *102*, 1995.
(40) (a) Spikes, G. H.; Sproules, S.; Bill, E.; Weyhermüller, T.; Wieghardt, K. *Inorg. Chem.* **2008**, *47*, 10935. (b) Spikes, G. H.; Bill, E.; Weyhermüller, T.; Wieghardt, K. *Angew. Chem., Int. Ed.* **2008**, *47*, 2973.
(41) (a) Witwicki, M.; Jerzykiewicz, M.; Jaszewski, A. R.; Jezierska, J.; Ozarowski, A. *J. Phys. Chem. A* **2009**, *113*, 14115. (b) Sebbar, N.; Bockhorn, H. *J. Phys. Chem. A* **2005**, *109*, 2223. (c) Barnard, G. M.; Brown, M. A.; Mabrouk, H. E.; McGarvey, B. R.; Tuck, D. G. *Inorg. Chim. Acta* **2003**, *349*, 142.
(42) The manuscript is under preparation.